ARTICLE

doi:10.1038/nature22071

Whole-genome landscapes of major melanoma subtypes

Nicholas K. Hayward[1,2]*§, James S. Wilmott[1,3]*, Nicola Waddell[2,4]*, Peter A. Johansson[2]*, Matthew A. Field[5], Katia Nones[2,4], Ann-Marie Patch[2,4], Hojabr Kakavand[3], Ludmil B. Alexandrov[6], Hazel Burke[1], Valerie Jakrot[1], Stephen Kazakoff[2,4], Oliver Holmes[2,4], Conrad Leonard[2,4], Radhakrishnan Sabarinathan[7,8], Loris Mularoni[7,8], Scott Wood[2,4], Qinying Xu[2,4], Nick Waddell[4], Varsha Tembe[9], Gulietta M. Pupo[9], Ricardo De Paoli-Iseppi[3], Ricardo E. Vilain[3], Ping Shang[3], Loretta M. S. Lau[10], Rebecca A. Dagg[11], Sarah-Jane Schramm[9], Antonia Pritchard[2], Ken Dutton-Regester[2], Felicity Newell[2], Anna Fitzgerald[12], Catherine A. Shang[12], Sean M. Grimmond[13], Hilda A. Pickett[10], Jean Y. Yang[14], Jonathan R. Stretch[1], Andreas Behren[15], Richard F. Kefford[1,16], Peter Hersey[1,17], Georgina V. Long[1,18], Jonathan Cebon[15], Mark Shackleton[19], Andrew J. Spillane[1], Robyn P. M. Saw[1], Núria López-Bigas[7,8,20], John V. Pearson[2,4]§, John F. Thompson[1]§, Richard A. Scolyer[1,3,21]§ & Graham J. Mann[1,9]§

Melanoma of the skin is a common cancer only in Europeans, whereas it arises in internal body surfaces (mucosal sites) and on the hands and feet (acral sites) in people throughout the world. Here we report analysis of whole-genome sequences from cutaneous, acral and mucosal subtypes of melanoma. The heavily mutated landscape of coding and non-coding mutations in cutaneous melanoma resolved novel signatures of mutagenesis attributable to ultraviolet radiation. However, acral and mucosal melanomas were dominated by structural changes and mutation signatures of unknown aetiology, not previously identified in melanoma. The number of genes affected by recurrent mutations disrupting non-coding sequences was similar to that affected by recurrent mutations to coding sequences. Significantly mutated genes included *BRAF*, *CDKN2A*, *NRAS* and *TP53* in cutaneous melanoma, *BRAF*, *NRAS* and *NF1* in acral melanoma and *SF3B1* in mucosal melanoma. Mutations affecting the *TERT* promoter were the most frequent of all; however, neither they nor *ATRX* mutations, which correlate with alternative telomere lengthening, were associated with greater telomere length. Most melanomas had potentially actionable mutations, most in components of the mitogen-activated protein kinase and phosphoinositol kinase pathways. The whole-genome mutation landscape of melanoma reveals diverse carcinogenic processes across its subtypes, some unrelated to sun exposure, and extends potential involvement of the non-coding genome in its pathogenesis.

Melanoma genomes have the highest mutation load of any cancer[1,2] and a predominant C>T nucleotide transition signature attributable to ultraviolet radiation[1]. However, some melanomas lack this signature and have fewer point mutations[3,4]. Melanomas driven by non-ultraviolet radiation are uncommon in cutaneous sites, but dominate those occurring in eyes, mucosal surfaces and acral (hands and feet) sites; the last type account for a much higher proportion of melanomas in Asians[5] than Europeans. Elucidating mutational processes and genomic drivers in all subtypes is key to further progress in melanoma epidemiology, prevention and targeted treatment globally.

The Cancer Genome Atlas (TCGA) study of 333 melanomas[2] excluded acral, mucosal and ocular subtypes and used exome and low-pass whole-genome sequencing (WGS). Examination of mutational process signatures, and of structural changes that drive melanoma, was restricted, and mutations outside the exome were not surveyed. Other sequencing studies have included acral and mucosal melanomas[6,7], but have been limited by sample size and/or restriction to exome sequencing.

We present the first large, high-coverage WGS study of melanomas from cutaneous, acral and mucosal sites, revealing distinct mutation processes, profiles and drivers across subtypes, the landscape of non-coding mutations, and paradoxical relationships between telomere maintenance gene mutations and telomere length. Mutational signatures of ultraviolet radiation exposure dominated cutaneous melanomas, while structural variants formed most aberrations in acral and mucosal melanomas. These last subtypes fundamentally differ in pathogenesis and therapeutic targets from cutaneous melanoma.

Study sample and mutation burden

The 183 melanoma samples comprised 75 primary tumours, 93 metastases and 15 cell lines derived from metastases; 35 were acral melanomas (arising from palms, soles or nail beds of the hands or feet), eight were

[1]Melanoma Institute Australia, The University of Sydney, North Sydney, Sydney, New South Wales 2065, Australia. [2]QIMR Berghofer Medical Research Institute, Brisbane, Queensland 4006, Australia. [3]Discipline of Pathology, Sydney Medical School, The University of Sydney, Sydney, New South Wales 2006, Australia. [4]Queensland Centre for Medical Genomics, Institute for Molecular Bioscience, University of Queensland, Brisbane, Queensland 4072, Australia. [5]Australian Institute of Tropical Health and Medicine, James Cook University, Cairns, Queensland 4878, Australia. [6]Los Alamos National Laboratory, Los Alamos, New Mexico 87545, USA. [7]Research Program on Biomedical Informatics, IMIM Hospital del Mar Medical Research Institute, Universitat Pompeu Fabra, 08003 Barcelona, Catalonia, Spain. [8]Institute for Research in Biomedicine (IRB Barcelona), The Barcelona Institute of Science and Technology, 08028 Barcelona, Spain. [9]Centre for Cancer Research, Westmead Institute for Medical Research, The University of Sydney, Westmead, Sydney, New South Wales 2145, Australia. [10]Children's Medical Research Institute, The University of Sydney, Westmead, Sydney, New South Wales 2145, Australia. [11]Children's Hospital at Westmead, The University of Sydney, Westmead, New South Wales Sydney, 2145, Australia. [12]Bioplatforms Australia, North Ryde, Sydney, New South Wales 2109, Australia. [13]University of Melbourne Centre for Cancer Research, University of Melbourne, Parkville, Melbourne, Victoria 3052, Australia. [14]School of Mathematics and Statistics, The University of Sydney, Sydney, New South Wales 2006, Australia. [15]Olivia Newton-John Cancer Research Institute, La Trobe University, Austin Health, Heidelberg, Melbourne, Victoria 3084, Australia. [16]Macquarie University, North Ryde, Sydney, New South Wales 2109, Australia. [17]Centenary Institute, The University of Sydney, Sydney, New South Wales 2006, Australia. [18]Department of Medical Oncology, Royal North Shore Hospital, St Leonards, Sydney, New South Wales 2065, Australia. [19]Peter MacCallum Cancer Centre and University of Melbourne, Melbourne, Victoria 3000, Australia. [20]Institució Catalana de Recerca i Estudis Avançats (ICREA), 08010 Barcelona, Spain. [21]Tissue Pathology and Diagnostic Oncology, Royal Prince Alfred Hospital, Camperdown, Sydney, New South Wales 2050, Australia.

*These authors contributed equally to this work.

§These authors jointly supervised this work.

© 2017 Macmillan Publishers Limited, part of Springer Nature. All rights reserved.

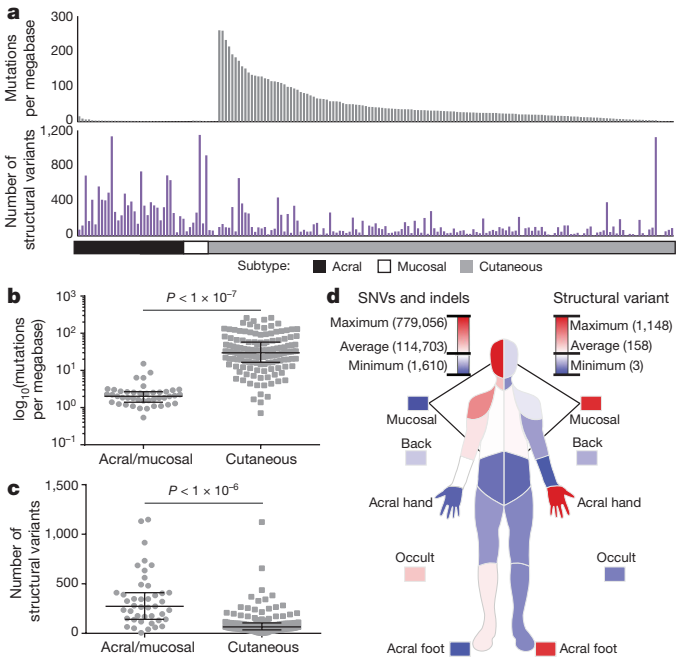

Figure 1 | Mutation burden. a, Rate of substitution/indel (SNV, top) and structural variant (bottom) mutations. **b**, Differences in SNV frequency by subtype (*t*-test, $P < 1 \times 10^{-7}$): acral and mucosal melanomas ($n = 43$) carried more than 18-fold fewer mutations than cutaneous melanomas ($n = 140$). **c**, Differences in structural variant frequency by subtype (*t*-test, $P < 1 \times 10^{-6}$): more structural variants in acral and mucosal than cutaneous melanomas. **d**, Relative abundance of aberrations by body site of the antecedent primary tumour. Highest (red) average SNV counts occurred in sun-exposed areas; highest structural variant counts occurred in sun-shielded body sites of mucosal and acral origin.

mucosal and the remainder cutaneous (Supplementary Table 1). WGS identified 20,894,255 substitutions (range 1,610–777,275 per tumour) and 96,467 small insertions/deletions (indels) (range 0–10, 114 per tumour) at an average rate of 38.23 mutations per megabase (range 0.54–260 mutations per megabase) (Supplementary Table 1 and Fig. 1), the 156,770 coding mutations (range 19–5,536 per tumour) comprising 0.8% (Supplementary Table 2). Single-nucleotide variant (SNV) and indel frequencies varied by melanoma subtype (*t*-test, $P < 1 \times 10^{-7}$), with >18 times more of these mutations in cutaneous (mean 49.17 mutations per megabase, range 0.71–259.69 mutations per megabase) than in acral and mucosal melanomas (mean 2.64 mutations per megabase, range 0.54–15.25 mutations per megabase) (Fig. 1b). Somatic structural variants were more frequent in acral and mucosal (mean 342.40, range 6–1,148) than in cutaneous melanomas (mean 101, range 3–1,123) (*t*-test, $P < 1 \times 10^{-6}$) (Fig. 1c, d). Greater proportions of the acral and mucosal melanoma genomes showed copy number variation, as in previous exome sequencing[3]; more regions were amplified (Mann–Whitney *U*-test, $P < 1.46 \times 10^{-4}$) and more genomes were aneuploid (χ^2 test, $P = 0.049$) than in cutaneous melanomas (Extended Data Fig. 1).

Mutation spectra and ultraviolet radiation

An algorithm using the sequence context of each mutation[1] identified 12 signatures, which varied considerably by melanoma subtype (Fig. 2a–c). Most melanomas (total $n = 139$; 136 cutaneous) were dominated by three novel signatures of ultraviolet radiation exposure (signatures 7a, 7b and 7c), recapitulating ultraviolet radiation signature 7 previously identified by exome sequencing[1] (Extended Data Fig. 2). The predominantly C>T substitutions at TpC dinucleotides (mutated base underlined) of signature 7a are probably due to repair of 6,4-photoproducts[8]. Signature 7b involves C>T substitutions at CpC and CpC, characteristic of cyclobutane pyrimidine dimers[8]. Signature 7c has high levels of T>C and T>A mutations, potentially caused by indirect DNA damage after ultraviolet radiation. Forty-four tumours, comprising 40 acral or mucosal melanomas and four cutaneous, all from infrequently sun-exposed sites, showed striking differences from the ultraviolet radiation-dominant group (Fig. 2). Six of nine signatures observed in this group have been described in other cancers[9] but never previously in melanoma and are presumably unrelated to ultraviolet radiation exposure. The most frequent were signature 1, the result of endogenous spontaneous deamination of 5-methylcytosine, and signature 5, ubiquitous in cancers of many types and of unknown aetiology[10] (Extended Data Fig. 2). Signature 13, attributed to activity of AID/APOBEC cytidine deaminases, occurred in 52 samples (28%) and all melanoma subtypes. Signatures 8, 17 and 18, of unknown aetiology, occurred in all melanoma subtypes at a combined frequency of 7–28%. Signature 6, associated with defective mismatch repair, was seen in the single cutaneous melanoma with a high MSIsensor[11] score.

Structural variants, telomere length

The combined frequency of all structural variants (deletions, duplications, tandem duplications and foldback inversions), was higher in acral and mucosal melanomas than in cutaneous melanomas (*t*-test, $P < 1 \times 10^{-6}$) (Fig. 1c and Supplementary Table 3). Acral and mucosal melanomas exhibited substantially more clusters of breakpoints, indicating more frequent complex rearrangements such as breakage–fusion–bridge (BFB) and chromothripsis (Extended Data Fig. 3a). We detected complex rearrangements including BFB-like in 18% ($n = 32$) of tumours, most of which ($n = 20$, 63%) were acral or mucosal melanomas (Extended Data Figs 4 and 5).

WGS provided the first opportunity to assess effects of mutagenic processes and driver mutation profiles of melanoma on immortalization via telomere length[12,13] (Methods and Extended Data Fig. 6b). Telomere length varied widely among the 183 samples, ranging from sixfold shorter to tenfold longer than the matched normal for each patient (Extended Data Fig. 6a). Telomere length was not correlated with melanoma subtype (Extended Data Fig. 6c), chromothripsis or BFB events (Extended Data Fig. 3).

Non-coding mutations

All mutations were annotated for genomic context including regulatory, untranslated and protein coding regions, the first such comprehensive survey in melanoma and one of the first in any cancer. *TERT* promoter mutations[14,15] were most common (Sanger sequencing), with 115 of 167 (69%) overall and 86% of cutaneous melanomas mutated at one or more of four positions upstream of the initiation codon (Extended Data Fig. 6d). These mutations created new binding sites for the E26 transformation-specific (ETS) family transcription factor GA-binding protein (GABP)[16], and were mutually exclusive with the exception of two samples with extremely high mutation burdens. In keeping with previous findings for acral melanoma[17], these mutations were less prevalent in acral and mucosal melanomas (4 of 38: 11%), accounting for their association with lower structural variant and higher SNV burden (Fisher's exact test, $P < 1 \times 10^{-17}$). There was no association between *TERT* promoter and *BRAF* mutation (χ^2 test, $P > 0.09$), in contrast to previous reports[18].

These putatively activating *TERT* promoter mutations were associated with modestly reduced telomere length (Mann–Whitney *U*-test, $P = 0.0022$) (Extended Data Fig. 6e–g). Telomere elongation in cancer depends either on *TERT* or a process of alternative lengthening of telomeres[19], often driven by mutations in *ATRX*[20]. The mutations in *ATRX* occur mutually exclusively with *TERT* promoter mutations in glioblastoma[21]. Ten melanomas (all cutaneous) had predicted loss-of-function mutations in *ATRX*, including two nonsense mutations, but paradoxically nine of these tumours also carried mutations in the *TERT* promoter and there was no association between *ATRX* mutation and telomere length (data not shown). Therefore, mutational activation of *TERT* does not simply facilitate telomere length extension, and the

© 2017 Macmillan Publishers Limited, part of Springer Nature. All rights reserved.

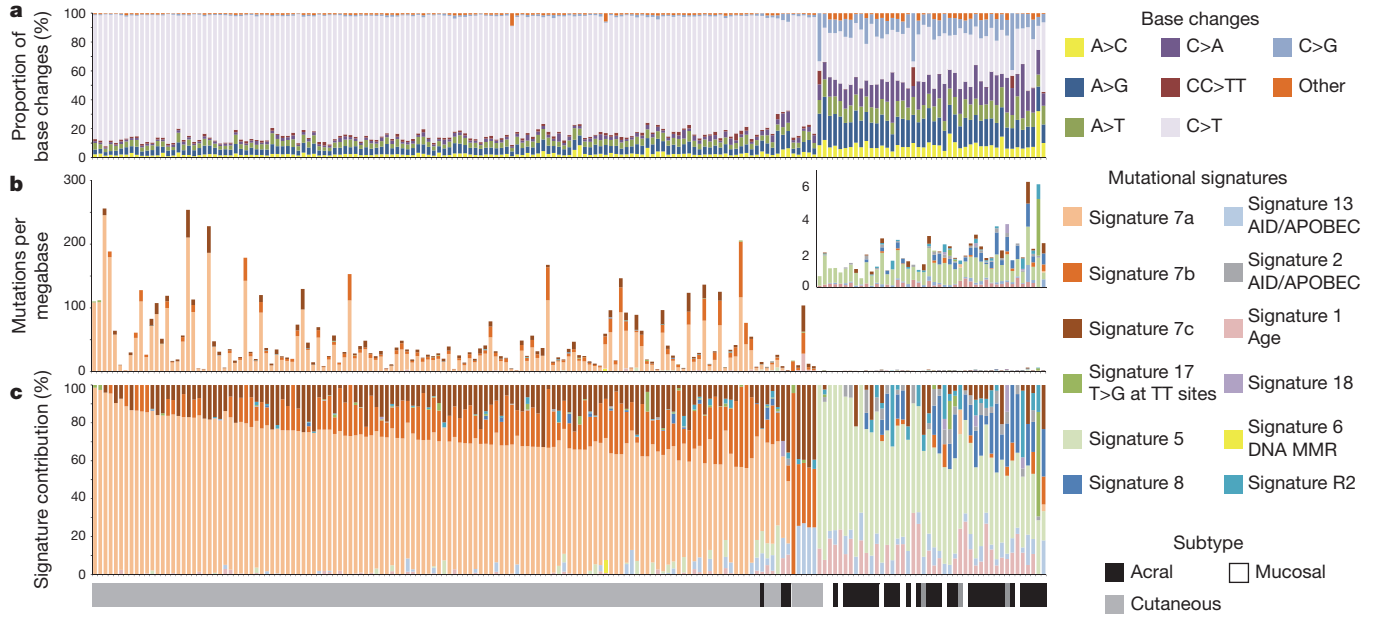

Figure 2 | Mutational processes. a, Proportion of somatic base changes: melanomas segregate into two groups with nearly all cutaneous melanomas showing a high proportion of C>T transitions. **b**, **c**, Twelve mutational signatures shown as (**b**) mutations per megabase and (**c**) percentage. Cutaneous melanomas ($n = 140$) were dominated by three novel ultraviolet radiation signatures, whereas melanomas with low mutation burden (acral or mucosal, $n = 43$) were dominated by signature 1 (associated with age), signature 5 (aetiology unknown and ubiquitous in diverse cancers) and signature 8 (seen in medulloblastoma and breast cancer).

relationships between alternative telomere maintenance mechanisms, telomere length and immortalization in melanoma must be complex.

All genes with recurrent mutations in the promoter, 5′ untranslated region (UTR) or 3′ UTR are listed (Supplementary Tables 4–6). To detect non-coding elements with an accumulation of functional mutations we used OncodriveFML[22], which detects signals of positive selection in mutations of coding and non-coding elements. Because of the high mutation rate at active transcription factor binding sites (TFBS) in melanoma[23], we used a version of OncodriveFML (version 1.1) that permuted mutations locally to assess whether the mutations observed disrupted or created TFBS more often than expected by chance. Promoter regions of nine genes were significantly ($q < 0.25$) biased towards high-impact mutations: creating new TFBS in *BLCAP*, *KBTBD8*, *TERT* and *ZNF778*, disrupting them in *NSUN6* and *RNF185*, and with other impacts in *RALY*, *RPL29* and *RPS27* (Supplementary Table 4). Only in the case of *TERT* (as previously reported[15]), *RNF185* and *RPS27* was an effect of these mutations on gene expression supported. In a further six genes with five or fewer occurrences of a promoter mutation (*NUDT10*, *PNPLA2*, *CCP110*, *UAP1*, *UBAC2* and *ZWINT*) OncodriveFML predicted creation of novel TFBS; however, too few tumours had such mutations for expression comparisons with wild-type tumours to be informative.

Recurrent mutations in the promoter of *NFKBIE* were present in 10 of 183 (5%) tumours including 3 of 9 desmoplastic melanomas[24]. The commonest (chr6:44233400) occurred in five melanomas, all cutaneous but lacking a desmoplastic component (Extended Data Fig. 7b). Mutations at this and one other position (chr6:44233417) have been reported previously, but the other four sites are novel (Extended Data Fig. 7b) and presumably lie outside the captured exome in the previous study. *NFKBIE* promoter mutations are thus enriched in desmoplastic melanomas (Fisher's exact test, $P < 0.0084$), but are also potential drivers of other cutaneous melanomas.

The most frequent 5′ UTR hotspot mutation, detected in 19 of 183 samples, was at the transcription start site of *RPS27* (chr1:153963239 C>T)[2,25] and a dinucleotide mutation was detected in one patient (chr1:153963239–153963240 CT>TC). *RPS27* also had several recurrent promoter mutations (Extended Data Fig. 7c), none predicted to cause gain or loss of TFBS. Recurrent mutations also occurred in the 5′ UTR of *PES1* (Extended Data Fig. 7d), *RPS14*, *CHCHD2* and *MRPS31* (Supplementary Table 5), the last identified as a common hotspot coding mutation by TCGA[2]. The 5′ UTR regions of *ERGIC3*, *PSMD8* and *TGS1* were significantly biased towards high functional impacting mutations and were expressed in most tumours; however, none showed expression differences associated with mutation status so their significance as drivers remains uncertain.

TCGA did not report 3′ UTR mutations; we observed recurrent ($n \geq 5$) 3′ UTR mutations in 18 genes (Supplementary Table 6). Only 11 of these genes were expressed in the tumour cohort and none has been associated with melanoma, except *PTPRT* which was recently reported to have frequent coding mutations[26].

Key coding mutations and TCGA genomic subgroups

Two tools were used to identify significantly mutated genes in each of the three melanoma subtypes (MutSigCV and OncodriveFML, $q < 0.1$; Supplementary Table 7). Four cutaneous melanoma significantly mutated genes were supported by both methods (*BRAF*, *CDKN2A*, *NRAS* and *TP53*), and five (*ARID2*, *CWH43*, *NF1*, *PTEN* and *RB1*) were supported by one method. *SF3B1* was identified as a significantly mutated gene, for the first time in mucosal melanoma, by OncodriveFML. In acral melanoma, OncodriveFML identified *BRAF*, *KIT*, *MAP2K2*, *NF1* and *NRAS* as significantly mutated genes.

Mutation frequencies of previously reported melanoma driver genes[2,3,26–30] varied considerably between melanoma subtypes. For example, no acral or mucosal melanomas had mutations in *TP53*, *PTEN*, *DDX3X*, *RASA2*, *PPP6C*, *RAC1* or *RB1*, indicating that the molecular pathways driving these melanoma subtypes differ markedly from those driving cutaneous melanoma. In line with previous studies[31], *KIT* mutations occurred more frequently in acral (3 of 35) and mucosal melanomas (2 of 8) than in cutaneous melanomas (6 of 140) (χ^2 test, $P < 0.044$). The distribution of mutations in selected melanoma genes (Supplementary Table 8) is shown in Fig. 3. Structural variants and copy number variation contributed heavily to the overall mutation frequency of some melanoma driver genes, especially *NF1*, *TP53*, *PTEN* and *KIT* (Extended Data Fig. 1b, c and Fig. 3). *BRAF* hotspot mutations were usually amplified, and these structural variants tended to involve *MET*, adjacent on chromosome 7. Similarly, *KIT* and

© 2017 Macmillan Publishers Limited, part of Springer Nature. All rights reserved.

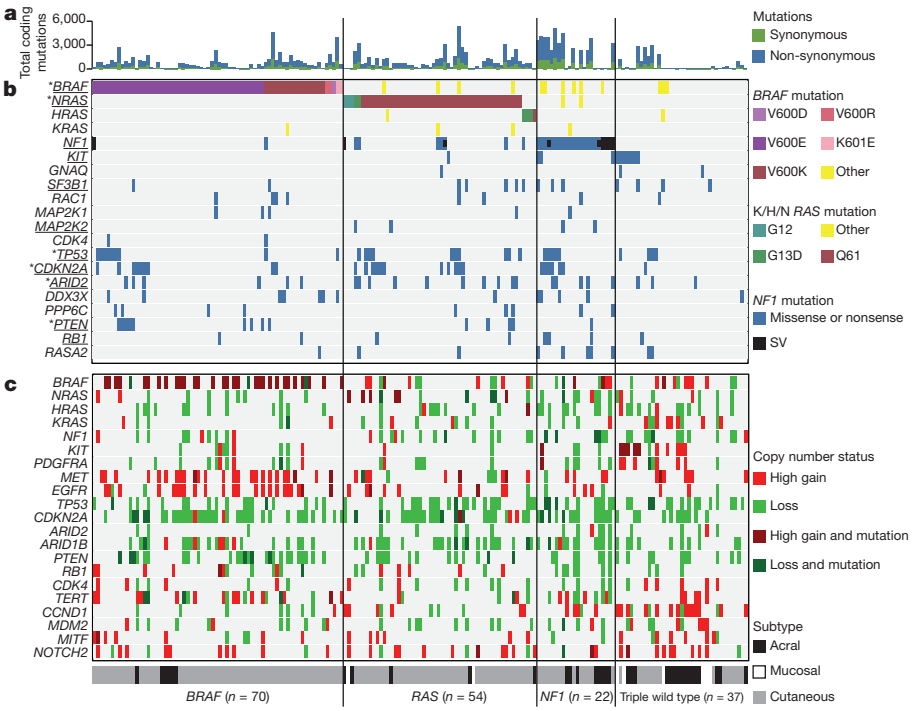

Figure 3 | Mutations and copy number changes in selected published melanoma driver genes. a, Somatic coding mutation rate. **b**, Mutations in significantly mutated genes (underlined) and selected published melanoma driver genes (Supplementary Table 8); *BRAF* and *RAS* aberrations coloured by mutation type; *genes differentially mutated between subtypes (Fisher's exact test, $P < 0.05$; missense, nonsense or structural variants (SV), or hotspot for *BRAF* and *RAS*), each in cutaneous more than in acral/mucosal melanoma. **c**, Copy number changes in selected melanoma-associated genes: loss (green), high gain (at least six copies, red). Melanoma subtype shown below.

PDGFRA, co-located within 0.35 megabases on chromosome 4, were frequently co-amplified. *MITF* amplifications were present in 10% of samples, and in all three melanoma subtypes. Many acral and mucosal melanomas had structural variants and high-level amplifications on the long arm of chromosome 11, often targeting *CCND1* (Extended Data Fig. 3c).

We analysed the genomic subgroups of melanoma proposed by TCGA: *BRAF* mutated, *RAS* mutated, *NF1* mutated or triple wild type[2] (Fig. 3a and Extended Data Figs 8 and 9). *NF1* aberrations occurred in 32 of 183 (17%) samples, and in 14 they were bi-allelic; 23 had point mutations/small indels only (15 nonsense, 4 missense, 3 splice site and 1 frameshift). Structural variants contributed heavily (Fig. 3b) to mutation burden in *NF1*, so previous studies in which structural variants were not assessed will have underestimated the *NF1*-mutated group and overestimated the proportion of triple wild-type melanomas. *NF1* mutation was found to co-occur with *RASA2* mutation (Fisher's exact test, $P < 0.003$), as recently described[29,32].

Most mucosal and acral ($n = 22$ of 43, 51%) melanomas, but only 15 of 140 (11%) cutaneous melanomas lacked *BRAF*, *NRAS* or *NF1* mutations; mutations in other cancer driver genes were frequent in this triple wild-type group, including loss-of-function mutations in *CDKN2A*, *TP53* and *ARID2*, and activating hotspot mutations in *GNAQ* and *SF3B1*. Notably, one *GNAQ* and three *SF3B1* mutations, commonly mutated in uveal[33,34] but not cutaneous melanoma[2], were found exclusively in four of six triple wild-type mucosal melanomas, marking an unappreciated set of driver genes and pathways shared by mucosal and uveal melanomas. Seven triple wild-type melanomas carried mutations in *KIT*, five of which had high-level amplifications. Triple wild-type melanomas had more focal amplifications of *KIT*, *CCND1*, *MDM2* and *KRAS* than did non-triple wild-type melanomas (Fisher's exact test, $P < 5.4 \times 10^{-5}$, 1.8×10^{-5}, 0.018 and 0.003, respectively).

Gene fusions

Gene fusions targeted several genes previously associated with melanoma (*RAF1* (ref. 35), *RAC1* (ref. 3), *MAP2K2* (ref. 36), *GRM3* (ref. 37), *MAP3K9* (ref. 30), *TRRAP*[38] and *PLCB4* (ref. 38)) (Supplementary Table 3) and known melanoma tumour suppressor genes: *NF1* ($n = 3$), *PARK2* ($n = 2$), *TP53*, *PTEN* and *PPP6C*. *RAF1* gene fusions, shown to increase MAP-kinase kinase (MEK) phosphorylation compared with wild-type RAF1, were observed in one triple wild-type and one *NF1*-mutated tumour[39]. The same *RAF1* exons were retained in both fusions, albeit fused to different genes (*CDH3* and *GOLGA4*) (Extended Data Fig. 9). In RNA sequencing of 44 samples, 17 of 136 potential fusion genes were expressed (Supplementary Table 3).

Fusions involved several kinase genes (Supplementary Table 3), the most frequently affected being *PAK1* ($n = 5$ samples: four acral melanomas, two of which were triple wild-type, and one cutaneous carrying a *BRAF* V600E mutation). These *PAK1* fusions are unlikely to be activating: the kinase domain was retained in four of five samples, in each case there was a different gene fusion partner (*AQP11*, *FCHSD2*, *TENM4*, *OR9Q1*) and two to four additional breakpoints within the *PAK1* gene. The next most frequently fused kinase gene was *DGKB*, with two fusions in acral triple wild-type melanomas and one in a cutaneous *BRAF* V600E mutated sample, each with multiple breakpoints within the *DGKB* gene with probable loss of function.

Signalling activation and clinical implications

All subtypes were dominated by mutations to the mitogen-activated protein kinase (MAPK) and phosphoinositol 3-kinase (PI3K) pathways, and receptor tyrosine kinase (RTK) (Supplementary Table 9 and Fig. 4b). The MAPK signalling pathway was enriched 1.34-fold (Fisher's exact test, $q < 1 \times 10^{-51}$) and bore mutations in 179 of 183 (98%) samples. Samples that harboured a mutated gene in both the MAPK and PI3K pathways had the highest proportion of phosphorylated (p-) ERK-positive tumour nuclei, whereas samples that were wild type for all genes in the PI3K and MAPK pathways had the lowest proportion (Fig. 4c, d). The highest p-AKT activation levels were seen in cases with only PI3K altered, whereas MAPK only and MAPK/PI3K wild-type cases had the lowest (differences not significant, one-way analysis of variance and post hoc Tukey's test).

Nearly all cutaneous (138 of 140, 99%) and most non-cutaneous (39 of 43, 91%) melanomas harboured a SNV/indel or structural variant breakpoint in one or more genes that can confer sensitivity to an agent that is approved by the US Food and Drug Administration or currently in a cancer clinical trial (Extended Data Fig. 10). The frequency of mutation and copy number variation of some potentially actionable genes (*CCND1*, *CCND2*, *KIT*, *KRAS*, *MDM2* and *PIP5K1A*) was significantly higher in non-cutaneous than cutaneous melanomas (two-proportion z-test, all $P < 0.05$).

© 2017 Macmillan Publishers Limited, part of Springer Nature. All rights reserved.

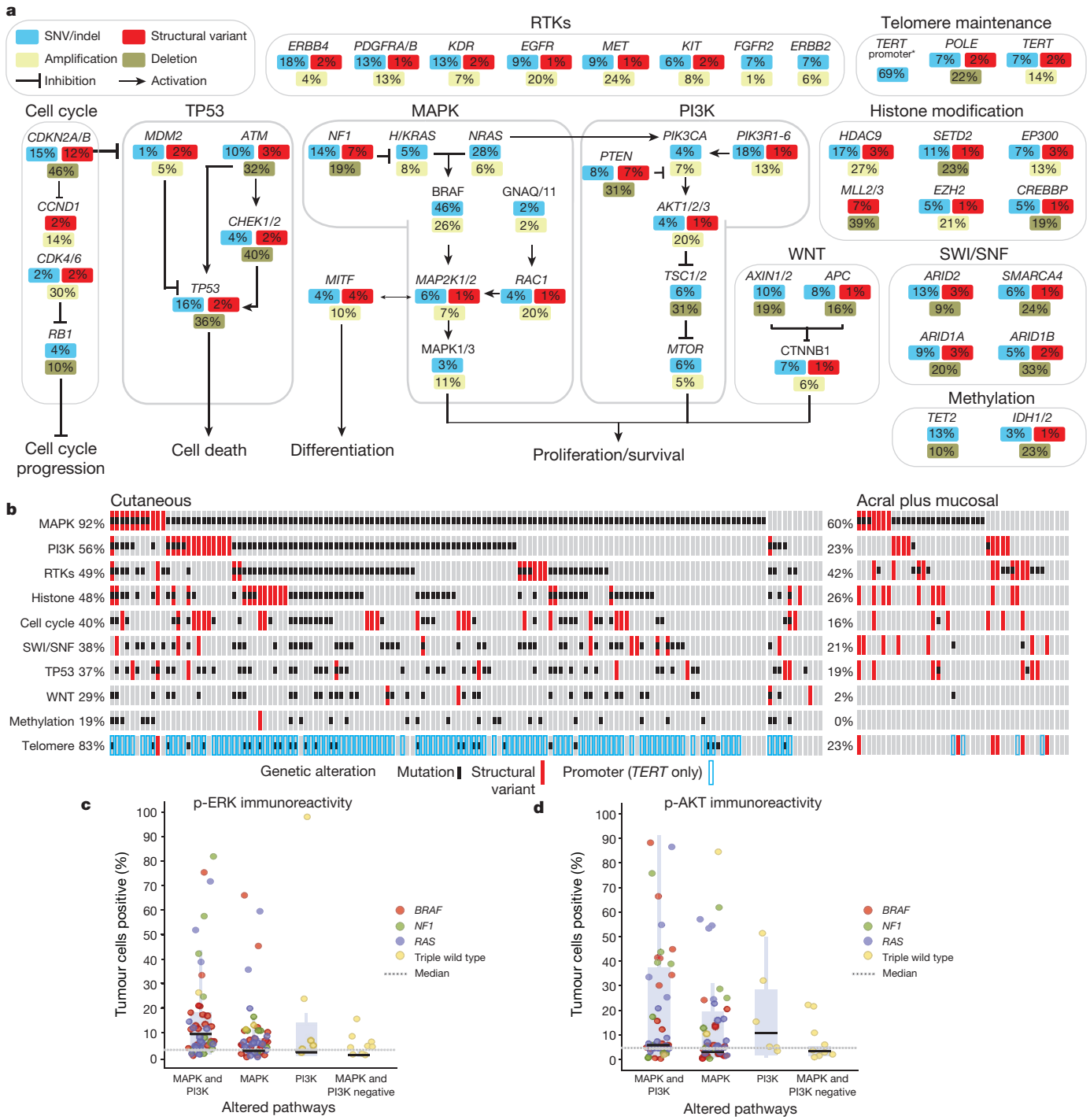

Figure 4 | Genes and signalling pathways recurrently altered in melanoma. a, Percentage of samples with protein-affecting aberrations in candidate driver genes, grouped by pathway: substitution/indels (blue), structural variants (red), copy number amplification (copy number > 5, yellow), homozygous deletion (green). **b**, Frequency of aberrations in pathways as percentage of cutaneous ($n = 140$) or non-cutaneous melanomas ($n = 43$). SWI/SNF, SWItch/Sucrose Non-Fermentable nucleosome remodeling complex. **c**, **d**, Percentage of tumour nuclei immunoreactive to p-ERK or p-AKT by multiplex-immunofluorescent staining; cases grouped according to mutated genes from the MAPK and PI3K pathways.

Discussion

This is the largest WGS analysis of melanoma so far and the largest to compare cutaneous, acral and mucosal subtypes. Acral and mucosal melanomas showed a markedly different genomic landscape from cutaneous melanoma, with a far lower mutation burden dominated by large-scale structural variants. Novel mutagen signatures in cutaneous melanomas probably reflect uncharacterized mechanisms of ultraviolet radiation damage. The principal mutation mechanisms driving mucosal and most acral melanomas were, in contrast, not attributable to ultraviolet radiation and imply novel carcinogenic exposures that are shared with cancers other than skin cancer. Notably, some mucosal melanomas exhibited significantly mutated genes (*GNAQ*, *SF3B1*) previously characteristic of uveal melanoma. In further contrast to cutaneous melanomas, acral and mucosal melanomas were infrequently driven by *TP53*, *PTEN* or *RB1* pathway lesions, and exhibited a variety of 'triple wild-type' mechanisms such as *KIT* mutations and focal amplifications of *KIT*, *CCND1*, *MDM2* and *KRAS*. Novel recurrently fused genes were also identified (*PAK1*, *DGKB*). Most cutaneous and non-cutaneous melanomas exhibited mutations in genes for which targeted therapies exist or are being evaluated in clinical trials.

© 2017 Macmillan Publishers Limited, part of Springer Nature. All rights reserved.

Non-coding mutations were surveyed for the first time at scale in melanoma, and their significance assessed taking into account the high mutation load at TFBS in melanoma[23]. The number of genes affected by recurrent non-coding mutations predicted to have a strong functional impact was equivalent to the number of genes affected by recurrent significant coding mutations. Eight genes in addition to *TERT* showed potential driver promoter mutations (*BLCAP*, *KBTBD8*, *NSUN6*, *RALY*, *RNF185*, *RPL29*, *RPS27* and *ZNF778*). Recurrent, probably functional 5′ UTR mutations were observed in *CHCHD2*, *PES1* and *RPS14*, as well as in genes previously reported as mutated (*RPS27*, *MRPS31*). Recurrent 3′ UTR mutations were common, and of uncertain significance, although *PTPRT* also carries frequent coding mutations[28].

Finally, we show the highly prevalent *TERT* promoter mutations in melanoma must confer selective advantage via dysregulation of telomere protection, whether by telomerase or the alternative lengthening of telomere mechanism, since they result in reduced, not increased, telomere length.

Online Content Methods, along with any additional Extended Data display items and Source Data, are available in the online version of the paper; references unique to these sections appear only in the online paper.

Received 22 November 2015; accepted 15 March 2017.
Published online 3 May 2017.

1. Alexandrov, L. B. *et al.* Signatures of mutational processes in human cancer. *Nature* **500,** 415–421 (2013).
2. Cancer Genome Atlas Network. Genomic classification of cutaneous melanoma. *Cell* **161,** 1681–1696 (2015).
3. Krauthammer, M. *et al.* Exome sequencing identifies recurrent somatic *RAC1* mutations in melanoma. *Nat. Genet.* **44,** 1006–1014 (2012).
4. Berger, M. F. *et al.* Melanoma genome sequencing reveals frequent *PREX2* mutations. *Nature* **485,** 502–506 (2012).
5. Chi, Z. *et al.* Clinical presentation, histology, and prognoses of malignant melanoma in ethnic Chinese: a study of 522 consecutive cases. *BMC Cancer* **11,** 85 (2011).
6. Furney, S. J. *et al.* Genome sequencing of mucosal melanomas reveals that they are driven by distinct mechanisms from cutaneous melanoma. *J. Pathol.* **230,** 261–269 (2013).
7. Furney, S. J. *et al.* The mutational burden of acral melanoma revealed by whole-genome sequencing and comparative analysis. *Pigment Cell Melanoma Res.* **27,** 835–838 (2014).
8. Ravanat, J. L., Douki, T. & Cadet, J. Direct and indirect effects of UV radiation on DNA and its components. *J. Photochem. Photobiol. B* **63,** 88–102 (2001).
9. Alexandrov, L. B., Nik-Zainal, S., Wedge, D. C., Campbell, P. J. & Stratton, M. R. Deciphering signatures of mutational processes operative in human cancer. *Cell Reports* **3,** 246–259 (2013).
10. Alexandrov, L. B. & Stratton, M. R. Mutational signatures: the patterns of somatic mutations hidden in cancer genomes. *Curr. Opin. Genet. Dev.* **24,** 52–60 (2014).
11. Niu, B. *et al.* MSIsensor: microsatellite instability detection using paired tumor-normal sequence data. *Bioinformatics* **30,** 1015–1016 (2014).
12. Mardin, B. R. *et al.* A cell-based model system links chromothripsis with hyperploidy. *Mol. Syst. Biol.* **11,** 828 (2015).
13. Nones, K. *et al.* Genomic catastrophes frequently arise in esophageal adenocarcinoma and drive tumorigenesis. *Nat. Commun.* **5,** 5224 (2014).
14. Horn, S. *et al.* TERT promoter mutations in familial and sporadic melanoma. *Science* **339,** 959–961 (2013).
15. Huang, F. W. *et al.* Highly recurrent TERT promoter mutations in human melanoma. *Science* **339,** 957–959 (2013).
16. Bell, R. J. *et al.* The transcription factor GABP selectively binds and activates the mutant TERT promoter in cancer. *Science* **348,** 1036–1039 (2015).
17. Liau, J. Y. *et al.* TERT promoter mutation is uncommon in acral lentiginous melanoma. *J. Cutan. Pathol.* **41,** 504–508 (2014).
18. Fredriksson, N. J., Ny, L., Nilsson, J. A. & Larsson, E. Systematic analysis of noncoding somatic mutations and gene expression alterations across 14 tumor types. *Nat. Genet.* **46,** 1258–1263 (2014).
19. Bryan, T. M., Englezou, A., Dalla-Pozza, L., Dunham, M. A. & Reddel, R. R. Evidence for an alternative mechanism for maintaining telomere length in human tumors and tumor-derived cell lines. *Nat. Med.* **3,** 1271–1274 (1997).
20. Ramamoorthy, M. & Smith, S. Loss of ATRX suppresses resolution of telomere cohesion to control recombination in ALT cancer cells. *Cancer Cell* **28,** 357–369 (2015).
21. Wiestler, B. *et al.* ATRX loss refines the classification of anaplastic gliomas and identifies a subgroup of *IDH* mutant astrocytic tumors with better prognosis. *Acta Neuropathol.* **126,** 443–451 (2013).
22. Mularoni, L., Sabarinathan, R., Deu-Pons, J., Gonzalez-Perez, A. & López-Bigas, N. OncodriveFML: a general framework to identify coding and non-coding regions with cancer driver mutations. *Genome Biol.* **17,** 128 (2016).
23. Sabarinathan, R., Mularoni, L., Deu-Pons, J., Gonzalez-Perez, A. & López-Bigas, N. Nucleotide excision repair is impaired by binding of transcription factors to DNA. *Nature* **532,** 264–267 (2016).
24. Shain, A. H. *et al.* Exome sequencing of desmoplastic melanoma identifies recurrent *NFKBIE* promoter mutations and diverse activating mutations in the MAPK pathway. *Nat. Genet.* **47,** 1194–1199 (2015).
25. Dutton-Regester, K. *et al.* A highly recurrent RPS27 5′UTR mutation in melanoma. *Oncotarget* **5,** 2912–2917 (2014).
26. Ding, L. *et al.* Clonal architectures and driver mutations in metastatic melanomas. *PLoS ONE* **9,** e111153 (2014).
27. Andersen, L. B. *et al.* Mutations in the neurofibromatosis 1 gene in sporadic malignant melanoma cell lines. *Nat. Genet.* **3,** 118–121 (1993).
28. Hodis, E. *et al.* A landscape of driver mutations in melanoma. *Cell* **150,** 251–263 (2012).
29. Krauthammer, M. *et al.* Exome sequencing identifies recurrent mutations in *NF1* and RASopathy genes in sun-exposed melanomas. *Nat. Genet.* **47,** 996–1002 (2015).
30. Stark, M. S. *et al.* Frequent somatic mutations in *MAP3K5* and *MAP3K9* in metastatic melanoma identified by exome sequencing. *Nat. Genet.* **44,** 165–169 (2011).
31. Curtin, J. A., Busam, K., Pinkel, D. & Bastian, B. C. Somatic activation of KIT in distinct subtypes of melanoma. *J. Clin. Oncol.* **24,** 4340–4346 (2006).
32. Arafeh, R. *et al.* Recurrent inactivating *RASA2* mutations in melanoma. *Nature Genet.* **47,** 1408–1410 (2015).
33. Harbour, J. W. *et al.* Recurrent mutations at codon 625 of the splicing factor *SF3B1* in uveal melanoma. *Nat. Genet.* **45,** 133–135 (2013).
34. Van Raamsdonk, C. D. *et al.* Frequent somatic mutations of *GNAQ* in uveal melanoma and blue naevi. *Nature* **457,** 599–602 (2009).
35. Palanisamy, N. *et al.* Rearrangements of the RAF kinase pathway in prostate cancer, gastric cancer and melanoma. *Nat. Med.* **16,** 793–798 (2010).
36. Nikolaev, S. I. *et al.* Exome sequencing identifies recurrent somatic *MAP2K1* and *MAP2K2* mutations in melanoma. *Nat. Genet.* **44,** 133–139 (2011).
37. Prickett, T. D. *et al.* Exon capture analysis of G protein-coupled receptors identifies activating mutations in *GRM3* in melanoma. *Nat. Genet.* **43,** 1119–1126 (2011).
38. Wei, X. *et al.* Exome sequencing identifies GRIN2A as frequently mutated in melanoma. *Nat. Genet.* **43,** 442–446 (2011).
39. Jones, D. T. *et al.* Oncogenic *RAF1* rearrangement and a novel *BRAF* mutation as alternatives to *KIAA1549:BRAF* fusion in activating the MAPK pathway in pilocytic astrocytoma. *Oncogene* **28,** 2119–2123 (2009).

Supplementary Information is available in the online version of the paper.

Acknowledgements This work was supported by Melanoma Institute Australia, Bioplatforms Australia, the New South Wales Ministry of Health, Cancer Council NSW, National Health and Medical Research Council of Australia (NHMRC), Cancer Institute NSW, Australian Cancer Research Foundation and the National Collaborative Research Infrastructure Strategy. N.K.H., Nicola W., R.A.S., J.S.W. and K.D.-R. were supported by NHMRC Fellowships, K.N. by a Keith Boden Fellowship, G.V.L. by the University of Sydney Medical Foundation, M.S. by Pfizer Australia, the Victorian Endowment for Knowledge, Science and Innovation and NHMRC, L.B.A. by a J. Robert Oppenheimer Fellowship at Los Alamos National Laboratory, and N.L.-B. by the European Research Council (Consolidator Grant 682398). Biobanking was supported by Melanoma Institute Australia, the Victorian Cancer Agency, Victorian Cancer Biobank, Victorian State Government Operational Infrastructure Support Program, Melanoma Research Alliance and the Melbourne Melanoma Project, and the efforts of patients, clinicians and other staff at health services across Australia. Cell lines were provided via the ABN-Oncology group, supported by NHMRC. Research at Los Alamos National Laboratory was under the auspices of the National Nuclear Security Administration of the US Department of Energy; the Los Alamos National Laboratory Institutional Computing Program was supported by contract DE-AC52-06NA25396. We acknowledge the support of colleagues at Melanoma Institute Australia, Royal Prince Alfred Hospital, NSW Health Pathology, Westmead Institute for Medical Research, Peter MacCallum Cancer Centre and Olivia Newton-John Cancer Research Institute. We thank D. Stetner for computing assistance.

Author Contributions P.A.J., M.A.F., K.N., A.-M.P., L.B.A., A.P., S.K., O.H., C.L., S.W., Q.X., Nick W. K.D.-R. and F.N. analysed genomic data; V.J., P.S., H.K., R.D.P.-I., V.T., G.M.P. and H.B. collected, prepared and analysed samples and data; L.M.S.L., R.A.D. and H.A.P. validated telomere length; L.M., R.S. and N.L.-B. analysed selection on coding and non-coding mutations; A.F., C.A.S., J.Y.Y. and S.-J.S. supported design and planning; J.V.P., Nicola W. and S.M.G. developed and directed the analysis pipeline; J.F.T., M.S., A.B., J.C., J.R.S., R.F.K., P.H., G.V.L., A.J.S., R.P.M.S. and R.E.V. collected samples and data; N.K.H., J.S.W., P.A.J., Nicola W., R.A.S. and G.J.M. designed and directed the study, analysed data and wrote the manuscript, which all authors reviewed.

Author Information Reprints and permissions information is available at www.nature.com/reprints. The authors declare no competing financial interests. Readers are welcome to comment on the online version of the paper. Publisher's note: Springer Nature remains neutral with regard to jurisdictional claims in published maps and institutional affiliations. Correspondence and requests for materials should be addressed to G.J.M. (graham.mann@sydney.edu.au).

Reviewer Information *Nature* thanks R. Halaban and the other anonymous reviewer(s) for their contribution to the peer review of this work.

© 2017 Macmillan Publishers Limited, part of Springer Nature. All rights reserved.

METHODS

No statistical methods were used to predetermine sample size. The experiments were not randomized. The investigators were not blinded to allocation during experiments and outcome assessment.

Human melanoma samples. The fresh-frozen tissue and blood samples analysed in the current study were obtained from Australian melanoma biospecimen banks, including the Melanoma Institute Australia ($n = 160$), Australasian Biospecimen Network-Oncology Cell Line Bank QIMR-Berghofer Institute of Medical Research ($n = 15$; all lines authenticated by DNA profiling and tested for mycoplasma contamination), Ludwig Institute for Cancer Research ($n = 4$) and Peter MacCallum Cancer Centre/Victorian ($n = 4$) biospecimen banks. All tissues and bloods form part of prospective collection of fresh-frozen samples accrued with written informed patient consent and institutional review board approval. Fresh surgical specimens were macro-dissected and tumour tissues were procured (with as little contaminating normal tissue as possible) and snap frozen in liquid nitrogen within 1 h of surgery. All samples were pathologically assessed before inclusion into the study, with samples requiring greater than 80% tumour content and less than 30% necrosis to be included. All samples were independently reviewed by melanoma pathologists (R.A.S., R.E.V.) to confirm the presence of melanoma and qualification of the above criteria. Samples requiring tumour enrichment underwent macrodissection or frozen tissue coring (Cryoxtract, Woburn, Massachusetts, USA) using a marked haematoxylin and eosin slide as a reference.

The histopathology of all mucosal and acral samples was reviewed by R.A.S. to confirm the diagnosis. Acral melanomas were classified as occurring within acral skin of the palm of the hand, sole of the foot and under nail beds. The lack of hair follicles, thickened stratum corneum and clinical site was confirmed in all cases. Mucosal melanomas were defined as occurring in the mucosal membranes lining oral, respiratory, gastrointestinal and urogenital tracts. The haematoxylin and eosin slides of the primary melanomas were reviewed for all mucosal and acral samples, and any tumour that arose in the junction of the acral/mucosal and cutaneous skin was excluded. Occult/unknown primary melanomas were considered cutaneous, since their genome landscape is indistinguishable from that of melanomas arising in the skin[40].

DNA extractions. Tumour DNA was extracted using DNeasy Blood and Tissue Kits (69506, Qiagen), according to the manufacturer's instructions. Blood DNA was extracted from whole blood using Flexigene DNA Kits (51206, Qiagen). All samples were quantified using the NanoDrop (ND1000, Thermoscientific) and Qubit dsDNA HS Assay (Q32851, Life Technologies), and DNA size and quality were tested using gel electrophoresis. Samples with a concentration of less than 50 ng μl^{-1}, or absence of a high molecular mass band in electrophoresis gels, were excluded from further analyses.

WGS. WGS was performed on Illumina Hiseq 2000 instruments (Illumina, San Diego, California, USA) at three Australian sequencing facilities (Australian Genomic Research Facility, Ramaciotti Centre for Genomics, John Curtin School of Medical Research) and Macrogen (Geumcheon-gu, Seoul, South Korea). All facilities performed library construction using TruSeq DNA Sample Preparation kits (Illumina) according to the manufacturer's instructions. The subsequent 100 base pair (bp) pair-end libraries were sequenced using Truseq SBS V3-HS kits to average depth 85× (range 43–219×) in the tumour sample and 64× (range 30–214×) in the matched normal.

WGS processing and quality control. Sequence data were aligned to the GRCh37 assembly using multi-threaded BWA 0.6.2-mt, resulting in sorted lane level files in sequence alignment/mapping format which were compressed and converted to binary file (BAM) created by samtools 0.1.19. Sample-level merged BAMs, one each for matched germline and tumour samples, were produced by in-house tools and duplicate reads marked with Picard MarkDuplicates 1.97 (http://picard.sourceforge.net). Quality assessment and coverage estimation was performed by qProfiler and qCoverage (http://sourceforge.net/projects/adamajava). To test for the presence of sample or data swaps, all sequence data were assessed by qSignature for concordance at approximately 1.4 million polymorphic genomic positions including the genotyping array data where available.

Somatic mutation analysis. Somatic mutations and germline variants were detected using a dual calling strategy using qSNP[41] and GATK[42], and indels of 1–50 bp in length were called with Pindel[43]. All mutations were submitted to the International Cancer Genome Consortium[44] Data Coordination Centre. Mutations were annotated with gene consequence using Ensembl gene annotation with SnpEff. Somatic genes that were significantly mutated were identified using two approaches: MutSigCV and OncodriveFML 1.1 (ref. 22) using a threshold of $q < 0.1$. Significant non-coding elements were detected using OncodriveFML 1.1 (ref. 22).

Somatic copy number and ploidy were determined using the TITAN tool[45]. Structural variants were identified using the qSV tool and chromosomes containing highly significant non-random distributions of breakpoints were identified as previously described[46]. Chromosomes identified to have clustering of breakpoints were inspected against criteria for chromothripsis[47] and the BFB cumulative rearrangement model[48]. Chromosomes with high numbers of translocations were identified with a minimum threshold of ten translocation breakpoints per chromosome following manual review.

Mutational signatures were predicted in each sample using a published framework[1]. Essentially, the substitution mutations across the whole genome in all cases were analysed in context of the flanking nucleotides (96 possible trinucleotide combinations). Identified signatures were compared with other validated signatures and the frequency of each signature per megabase was determined.

Recurrent non-coding mutations. Statistical significance of recurrent non-coding mutations was estimated using a permutation test. A null distribution of recurrence was estimated by randomly shuffling all mutations within each sample and recording the number of recurrent mutations within the regions of interest. To take into account not only the varying mutation burden but also the different mutation signatures, we restricted the random shuffling such that the mutation in the middle of a trinucleotide, ABC, was only shuffled to the same trinucleotide.

Functional impact bias of mutations in promoters, 3′ UTRs and 5′ UTRs. Promoters and UTRs likely to play a role in tumorigenesis were identified with OncodriveFML[22], a framework able to detect signals of positive selection in both the coding and the non-coding regions of the genome by measuring the bias towards the accumulation of functional mutations. The functional impact of mutations in gene promoters was assessed using the CADD (Combined Annotation Dependent Depletion)[49], TFBS creation and TFBS disruption scores. The CADD scores measure the deleteriousness of mutations, and are calculated by integrating multiple annotations into a single metric by contrasting variants that survived natural selection with simulated mutations. The scores for TFBS creation (motif gain) and disruption (motif break) were computed by following the steps described in ref. 50. The score value indicates the difference between position weight matrix matching scores of the germline and mutant alleles. The 5′ UTRs were analysed using the TFBS disruption scores while 3′ UTRs were analysed using the CADD scores. The statistical significance of promoters and UTRs was derived by comparing the average functional impact score of the mutations in the element with the functional impact scores obtained by permuting 100,000-fold the observed mutations, maintaining their trinucleotide context. In addition, since the rate of somatic mutations in melanoma is highly increased at active TFBS[23], OncodriveFML was adapted (version 1.1) to perform a strictly local permutation in windows of 51 bp (25 nucleotides at each side of the mutation). This variation in the background model of OncodriveFML allowed us to better estimate whether the mutations observed in tumours disrupted or created TFBS more than expected by chance. The statistical significance of promoters and UTRs mutated in at least two samples was adjusted with the Benjamini–Hochberg correction for multiple testing.

We also used miRanda version 3.3a to predict whether the recurrent 3′ UTR mutations alter (disrupt or create) microRNA (miRNA) binding sites. The 50-base sequence surrounding each 3′ UTR was used as input to miRanda. miRNAs that were predicted to hit either the wild-type or mutant sequence (but not both) were considered potential targets and further filtered as follows. We required a hit to perfectly align against the seed region of the miRNA (nucleotides 2–8), that the mutation lay within the seed and that the predicted binding energy was higher (lower ΔG) in the non-hit than in the hit.

Telomere length estimation. To estimate telomere length, we counted telomere motifs in the whole gene data using the quantitative-PCR-validated qMotif tool (https://sourceforge.net/p/adamajava/wiki/qMotif) implemented in JAVA using the Picard library (version 1.110). qMotif is driven by a single plain-text configuration file in the 'Windows INI-file' style and the input is a WGS BAM file that has been duplicate-marked and coordinate-sorted. Essentially, qMotif uses a two-stage matching system where the first stage is a quick-but-strict string match and the second stage is a slower but more flexible regular expression match; only reads that pass stage 1 go on to the much slower match in stage 2. For telomere quantification, a string representing three concurrent repeats of the canonical telomere motif (TTAGGGTTAGGGTTAGGG) was used as the stage 1 match, and a simple pattern match for stage 2 which captured any read with two or more concurrent occurrences of the telomeric repeat with variation allowed in the first three bases. The relative tumour telomere length was then estimated by comparing the tumour read counts with the matched normal sample. Telomere length was validated by quantitative PCR[51].

Sanger sequencing of TERT promoter. Direct PCR amplification and Sanger sequencing were performed using the primers hTERT_F ACGAACGTGG CCAGCGGCAG and hTERT_R CTGGCGTCCCTGCACCCTGG, which amplify a 474 bp region of the *TERT* promoter[52]. PCR was done in a 13 µl volume containing 1 µl of 20 ng μl^{-1} gDNA, 1.25 µl of 10× $MgCl_2$, 2.5 µl betaine, 1.25 µl deoxynucleotides (2.5 mM), 1 µl of 10 µM primers and 0.25 µl of PFU Turbo (600250, Agilent). PCR reactions were performed under the following conditions: 95 °C for

© 2017 Macmillan Publishers Limited, part of Springer Nature. All rights reserved.

5 min, followed by four cycles of 95 °C for 30 s, annealing at 66 °C for 1 min and polymerization at 72 °C for 1 min. This was followed by 4 more cycles with a lowered annealing temperature of 64 °C for 1 min, followed by 28 cycles with annealing temperatures of 62 °C. Subsequent PCR products were sequenced on an AbiPrism 3130xl Genetic Analyzer (Applied Biosystems) and data analysed using Sequence Scanner Software 2 (Applied Biosystems) with reference to the sequences from the NCBI gene database, *TERT* (chr5:1295071–1295521).

Ultra-deep custom amplicon sequencing of non-coding mutations. Illumina TruSeq Custom Amplicon V1.5 was used to validate 20 recurrent non-coding point mutations in the promoter ($n = 11$), 3′ UTR ($n = 3$) and 5′ UTR ($n = 6$) regions of genes with frequent non-coding mutations in 164 of the 183 samples. Illumina DesignStudio (Illumina, San Diego, California, USA) was used to design 250 bp sequences of the target regions. Sequencing libraries were prepared using the TruSeq Custom Amplicon Library Preparation Guide and the TruSeq Custom Amplicon Index Kit, and sequenced on a MiSeq Illumina sequencer V2 (Illumina). Sequences were aligned to the reference genome (GRCh37/hg19) using BWA 0.6.2-mt. A pileup approach was used to determine the base count at each position of interest. A mutation was considered verified if the mutant allele frequency was >10%.

Exome sequencing. Exome capture was performed on 1 μg of DNA extracted from tumour and normal blood using an Illumina TruSeq Exome Library Prep Kit. Libraries were sequenced (paired-end sequencing) on an Illumina HiSeq2000 platform with a minimum coverage of 61× (normal) and 59× (tumour). Exome sequence data were produced for 53 patients in the cohort and used to validate coding mutations detected by WGS.

RNA extraction and sequencing. Total RNA was extracted from fresh-frozen tissue using a mirVana miRNA Isolation Kit (Applied Biosystems, AM1560). RNA quality and presence of a small RNA fraction were measured using the Agilent 2100 RNA 6000 Nano and small RNA kits. RNA sequencing was performed using 1 μg of total RNA, which was converted into messenger RNA libraries using an Illumina mRNA TruSeq kit. RNA sequencing was performed using 2 × 75 bp paired-end reads on an Illumina Hiseq2000. Small RNA sequencing was performed using 1 μg of total RNA, which was converted into a small RNA libraries, size selection range 145–160 bp (RNA of 18–33 nucleotides) using Illumina's TruSeq Small RNA Library Preparation Kit and sequenced on an Illumina Hiseq2000 using 50 bp single-read sequencing with 1% control spiked in.

RNA sequence reads were aligned to transcripts corresponding to ensemble 70 annotations using RSEM[53]. RSEM data were normalized using TMM (weighted trimmed mean of M-values) as implemented in the R package 'edgeR'. For downstream analyses, normalized RSEM data were converted to counts per million. Genes with at least 5 counts per million in at least two samples were considered expressed.

Body site distribution of SNV/indel and structural variants. Total numbers of SNV/indel and structural variants were compared according to primary melanoma body site, categorized into abdomen, acral hand, acral foot, back, lower arm, lower leg, mucosal, neck, shoulder, thorax, upper arm, upper leg, and face and scalp. Any samples with an unknown primary site or occult classification were excluded from analysis. Heat maps were produced in Spotfire-Tibco (version 6.0, http://spotfire.tibco.com) on the basis of the combined total number of SNV and indels, or by structural variants. A two-colour heat map (red high, blue low) was produced and colours were overlaid onto an adapted SVG human body diagram that was created using Adobe Illustrator CS6.

Clinically actionable gene mutations. The frequency of clinically actionable mutations was assessed by annotating genomic variants using the IntOGen Cancer Drivers Actionability database (2014), which identifies mutations that may confer sensitivity to therapeutic agents[54]. The database was used to assign an activating or loss-of-function role to mutated genes. Loss of heterozygosity, silent mutations, deletions to activating genes or amplifications to loss-of-function genes were not included in the analysis. Additionally, visual inspection using the Integrative Genome Viewer (IGV, Broad) was used to identify only high-confidence structural rearrangement breakpoints with clustered supporting reads with both discordant read pair and soft clipping evidence. Structural variants with a high incidence of random non-clustered background signal surrounding the breakpoints along with low numbers of supporting non-duplicate reads were excluded from analysis for this figure (Extended Data Fig. 10). The proportion of tumours with a mutation to a particular actionable gene was calculated and classified on the basis of mutation type into (1) SNV/indel, (2) SNV/indel and structural variant, (3) structural variant or (4) copy number variation only.

Commonly mutated genes and pathways. A hand-curated list of commonly mutated tumour suppressor genes and oncogenes was created and analysed for the frequency of mutation (Fig. 4a). Mutations were defined as SNV/indel, structural variant, copy number amplifications and copy number deletions. Loss of heterozygosity, silent mutations, RNA mutations, deletions to oncogenes or amplifications to tumour suppressor genes were not included in the figure. Structural variant breakpoints were subjected to manual inspection using the Integrative Genome Viewer (IGV, Broad) and only events confirmed as somatic and predicted to alter transcription processing were considered further. We then overlaid the alterations from Fig. 4a onto pathways defined by Kyoto Encyclopedia of Genes and Genomes (KEGG) and Gene Ontology (GO) gene sets from MSigDB version 5.0. A pathway was considered altered in a given sample if at least one gene in the pathway contained an SNV/indel or structural variant. The pathways were then stratified according to cutaneous or non-cutaneous subtypes. A mutation file with sample identities and their mutated pathways was entered for analysis into the OncoPrinter tool (http://cbioportal.org).

Multiplex-immunofluorescent staining. MAPK and PI3K pathway status was also assessed by multiplex-immunofluorescent staining for phosphorylated ERK and AKT (106/183). All immunohistochemical staining was performed on a Dako Autostainer Plus (Dako, Glostrup, Denmark) using a Dako Envision Flex detection kit (K8000, Dako) and OPAL 7-colour IHC Kit for visualization (NEL797B001KT, PerkinElmer). Consecutive staining rounds included p-AKT (1:100, NCL-L-Akt-Phos, Leica), p-ERK (1:1,600, CS4370, Cell Signalling) and SOX10 (1:800, ACI 3099A, Biocare). Multispectral quantitative image analysis was performed on a Vectra 3 slide scanner (PerkinElmer, USA). The captured multispectral images were analysed using the quantitative InForm image analysis software (PerkinElmer, USA).

Data deposition. All somatic variants for this study have been deposited in the International Cancer Genome Consortium Data Coordination Centre and are publicly available at https://dcc.icgc.org. The BAM files have been deposited in the European Genome-phenome Archive (https://www.ebi.ac.uk/ega/) with accession number EGAS00001001552.

Code availability. Tools used in this publication that were developed in-house are available from the SourceForge public code repository under the AdamaJava project (http://sourceforge.net/projects/adamajava/).

Data availability. Source data are provided or are available from the corresponding author upon reasonable request.

40. Dutton-Regester, K. *et al.* Melanomas of unknown primary have a mutation profile consistent with cutaneous sun-exposed melanoma. *Pigment Cell Melanoma Res.* **26,** 852–860 (2013).
41. Kassahn, K. S. *et al.* Somatic point mutation calling in low cellularity tumors. *PLoS ONE* **8,** e74380 (2013).
42. McKenna, A. *et al.* The Genome Analysis Toolkit: a MapReduce framework for analyzing next-generation DNA sequencing data. *Genome Res.* **20,** 1297–1303 (2010).
43. Ye, K., Schulz, M. H., Long, Q., Apweiler, R. & Ning, Z. Pindel: a pattern growth approach to detect break points of large deletions and medium sized insertions from paired-end short reads. *Bioinformatics* **25,** 2865–2871 (2009).
44. Hudson, T. J. *et al.* International network of cancer genome projects. *Nature* **464,** 993–998 (2010).
45. Ha, G. *et al.* TITAN: inference of copy number architectures in clonal cell populations from tumor whole-genome sequence data. *Genome Res.* **24,** 1881–1893 (2014).
46. Patch, A. M. *et al.* Whole-genome characterization of chemoresistant ovarian cancer. *Nature* **521,** 489–494 (2015).
47. Korbel, J. O. & Campbell, P. J. Criteria for inference of chromothripsis in cancer genomes. *Cell* **152,** 1226–1236 (2013).
48. Kinsella, M. & Bafna, V. Combinatorics of the breakage-fusion-bridge mechanism. *J. Computat. Biol.* **19,** 662–678 (2012).
49. Kircher, M. *et al.* A general framework for estimating the relative pathogenicity of human genetic variants. *Nat. Genet.* **46,** 310–315 (2014).
50. Fu, Y. *et al.* FunSeq2: a framework for prioritizing noncoding regulatory variants in cancer. *Genome Biol.* **15,** 480 (2014).
51. Lau, L. M. *et al.* Detection of alternative lengthening of telomeres by telomere quantitative PCR. *Nucleic Acids Res.* **41,** e34 (2013).
52. Griewank, K. G. *et al. TERT* promoter mutations are frequent in atypical fibroxanthomas and pleomorphic dermal sarcomas. *Mod. Pathol.* **27,** 502–508 (2014).
53. Li, B. & Dewey, C. N. RSEM: accurate transcript quantification from RNA-seq data with or without a reference genome. *BMC Bioinformatics* **12,** 323 (2011).
54. Rubio-Perez, C. *et al.* In silico prescription of anticancer drugs to cohorts of 28 tumor types reveals targeting opportunities. *Cancer Cell* **27,** 382–396 (2015).

© 2017 Macmillan Publishers Limited, part of Springer Nature. All rights reserved.

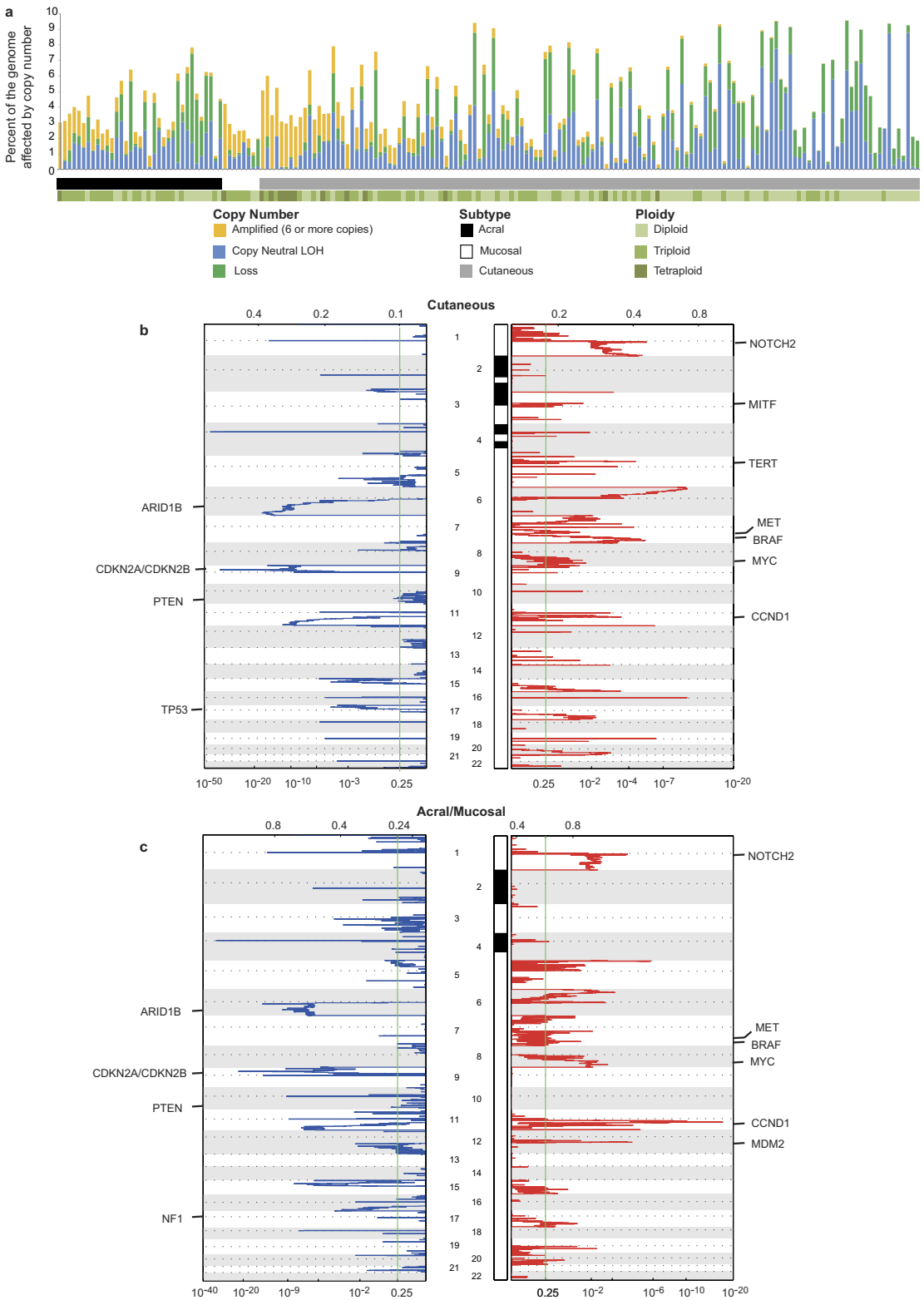

Extended Data Figure 1 | Copy number and ploidy in melanoma. **a**, The proportions of each of the melanoma genomes ($n = 183$) that were affected by loss (copy number 1 or 0), copy neutral loss of heterozygosity (LOH) and high gain (at least six copies) are shown in the histogram. The melanoma subtype and degree of ploidy are illustrated in the colour bar beneath the histogram. **b**, **c**, GISTIC analysis was performed to determine significant regions of recurrent copy number change in the cutaneous (**b**, $n = 140$) and acral and mucosal (**c**, $n = 43$) tumours.

© 2017 Macmillan Publishers Limited, part of Springer Nature. All rights reserved.

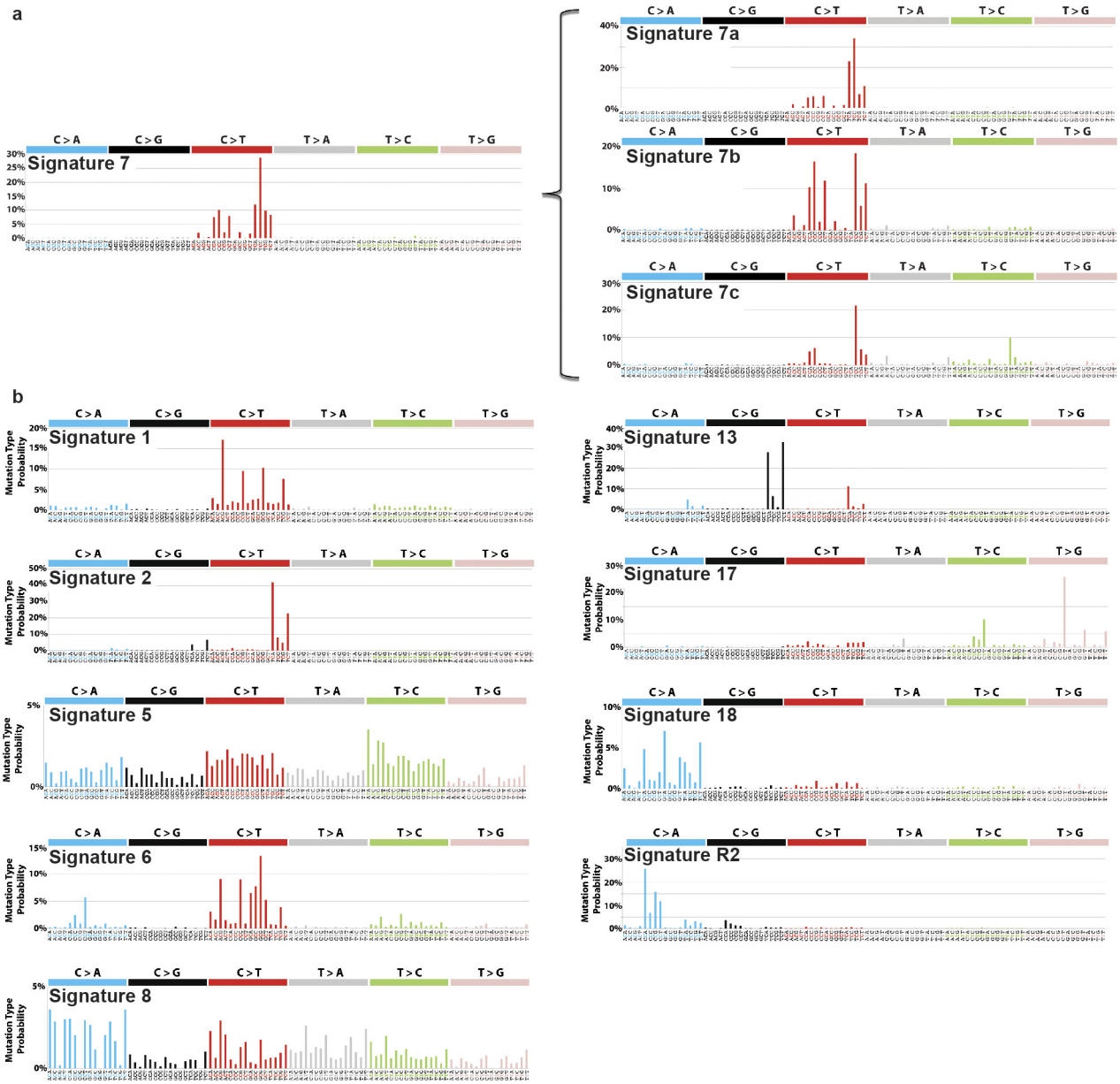

Extended Data Figure 2 | Mutation signatures in melanoma. Twelve mutation signatures in melanoma were identified taking into account the sequence context immediately before and after the mutation. Each signature is displayed showing the probability for each of the 96 mutation types. **a**, Three novel signatures, associated with ultraviolet radiation, were identified. These signatures perfectly recapitulate the ultraviolet radiation mutation signature previously extracted from exome sequencing data. Signature 7a is predominately C>T transitions occurring at TpC dinucleotides and, on the basis of similarity with the sequence context, it is most likely owing to the formation of 6,4-photoproducts. Signature 7b is described by C>T transitions at CpC dinucleotides. This sequence context is characteristic for the formation of cyclobutane pyrimidine dimers due to ultraviolet radiation exposure. Signature 7c has a high proportion of C>T substitutions, and high levels of T>C and T>A mutations, demonstrating the ability of ultraviolet radiation to generate both transitions and transversions. The underlying processes damaging DNA and resulting in signature 7c are currently unknown but they could potentially be due to indirect DNA damage. **b**, Of the nine non-ultraviolet radiation associated signatures, three (signatures 1, 5 and 17) have previously been observed in melanoma and six have been seen in other cancer types but not previously noted in melanoma. Signature 1 is the result of an endogenous mutational process initiated by spontaneous deamination of 5-methylcytosine and is associated with age of the patient. Signature 5 (aetiology unknown) was the dominant signature in tumours with no ultraviolet radiation signature; it is, together with signature 1, the most common signature, observed in diverse cancer types. Signature 17 (aetiology unknown) has been seen in melanoma previously and was here observed in 52 tumours (exclusively cutaneous and acrals). Signature 8 was one of the dominant signatures in tumours with no ultraviolet radiation signature (together with signatures 5 and 1); it has previously been observed in breast cancer and medulloblastoma and was evident in 39 melanomas. Signatures 2 and 13 have been attributed to activity of the AID/APOBEC family of cytidine deaminases and are often observed in the same samples; here, most non-ultraviolet samples showed both signatures, but the highest level of signature 2 was observed in a cluster of four samples in which signatures 2, 7a and 7c were observed. Signature 6 is associated with defective DNA mismatch repair and typically found in microsatellite-unstable tumours; it was observed in one melanoma in this cohort. Signature 18 has been observed frequently in neuroblastoma; it was identified in 13 melanomas. Signature R2 reflects a sequencing artefact.

© 2017 Macmillan Publishers Limited, part of Springer Nature. All rights reserved.

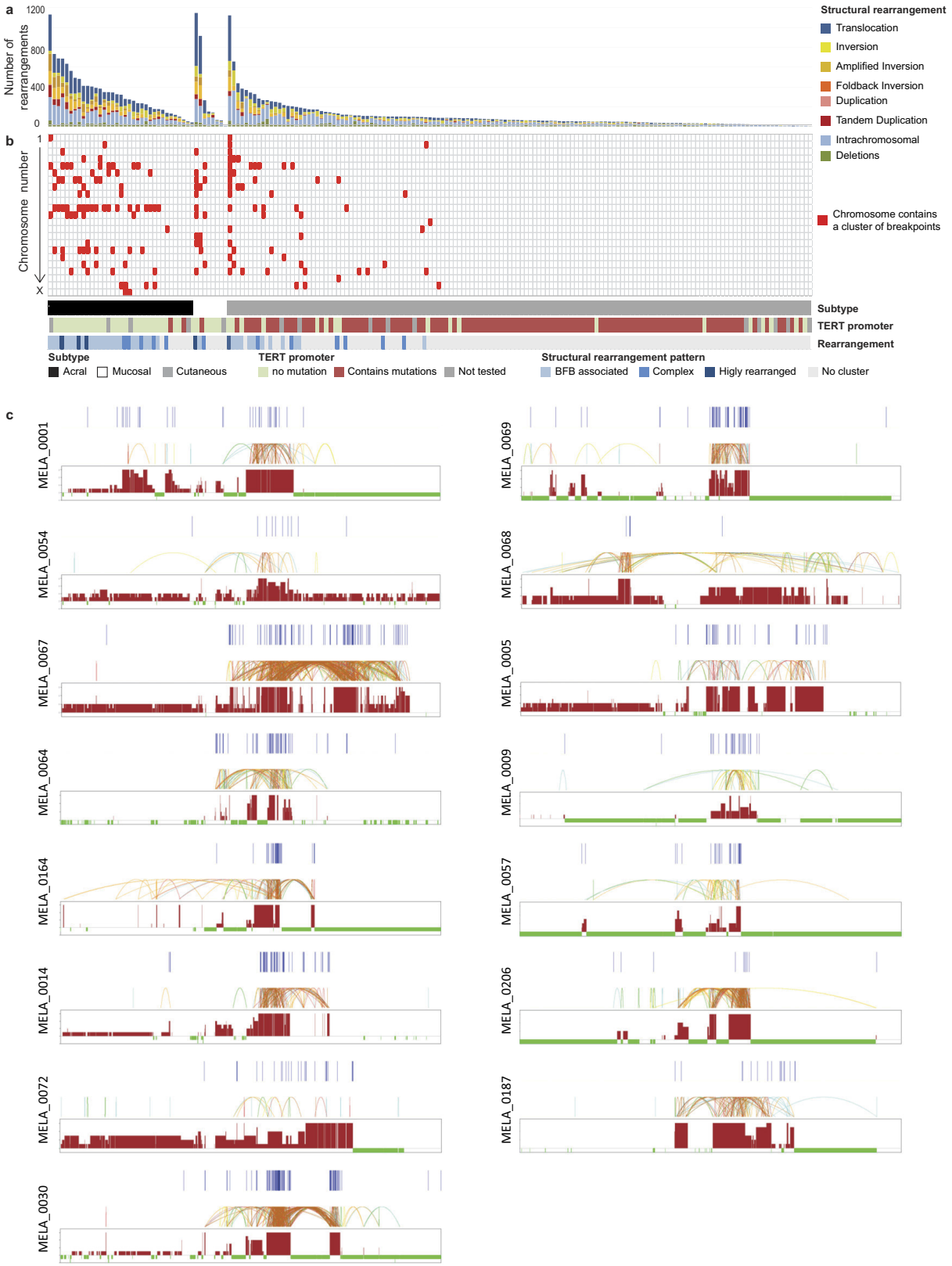

Extended Data Figure 3 | Structural variants clustering on chromosome 11 in acral melanoma. a, The number and type of structural variant is shown for each tumour ($n = 183$). **b**, Chromosomes containing complex rearrangements are shown in red defined as chromosomes with a clustered arrangement of breakpoints (Kolmogorov–Smirnov goodness of fit test, $P < 0.0001$) and a high density of breakpoints (number of breakpoints exceeds the extreme threshold value of the upper quartile plus 5× interquartile range for the chromosomal distribution of breakpoints). The observed pattern of breakpoint clusters and copy number events was used to classify tumours as BFB-associated, complex, highly rearranged or no clusters of events. *TERT* promoter mutations are also shown. **c**, Patterns of structural variants and copy number in all acral melanomas that contained a cluster of structural variants on chromosome 11. Graphs show the most frequent translocations and other structural variants (copy number in red, gain; in green, loss).

© 2017 Macmillan Publishers Limited, part of Springer Nature. All rights reserved.

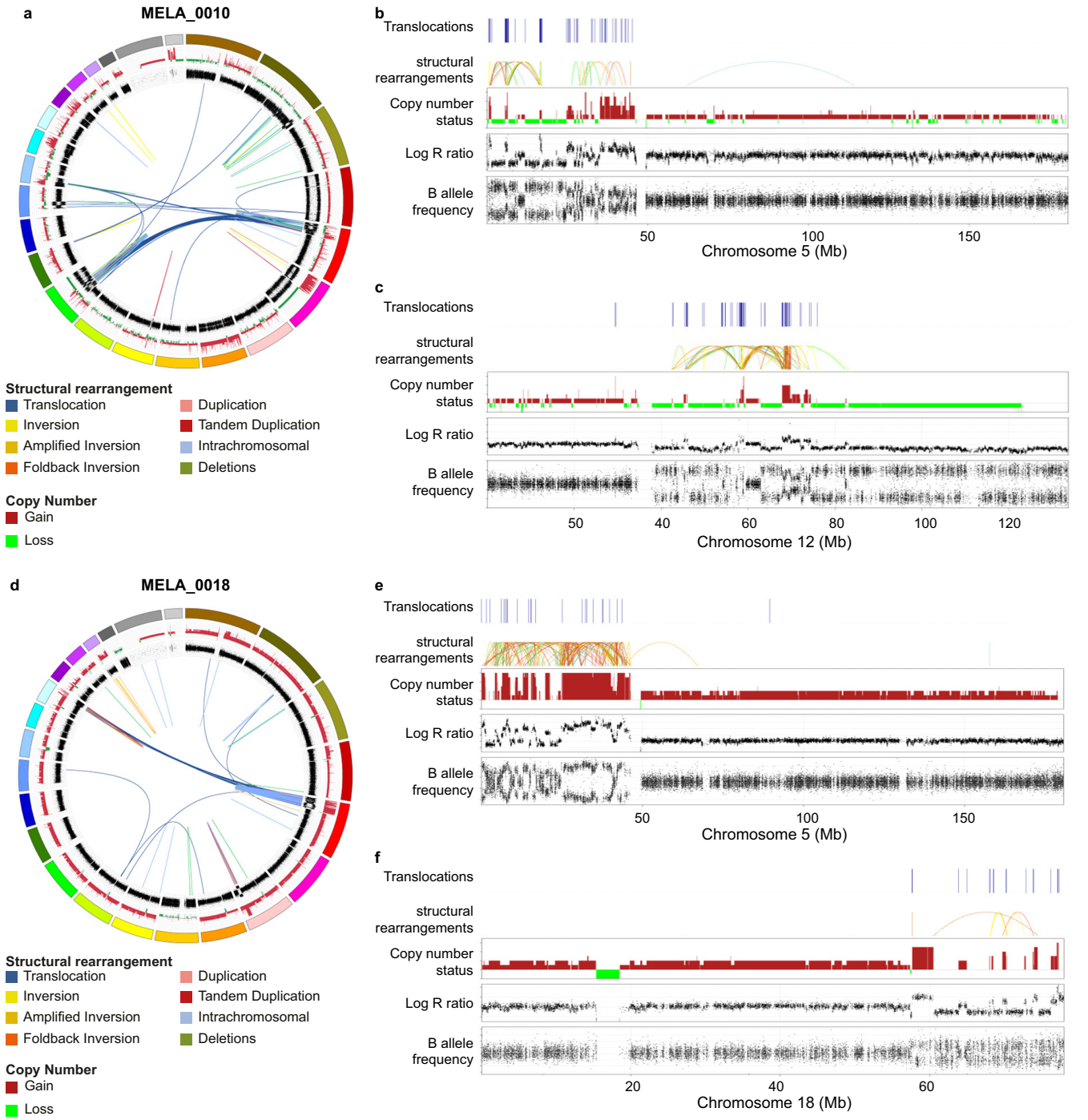

Extended Data Figure 4 | Fine structure of two structural variants. **a**, Circos plot of MELA_0010 shows a cluster of structural variants on chromosomes 5 and 12. The outer coloured ring on the Circos plot represents each chromosome, the next ring is the copy number (red, gain; green, loss), the inner ring is the B-allele frequency, and the structural variants are shown by the lines in the centre of the plot. **b**, The cluster of rearrangements on chromosome 5 in MELA_0010 are shown from top to bottom: translocations (blue), all other rearrangements, copy number status, log(R ratio) and B-allele frequency. **c**, The cluster of rearrangements on chromosome 12 in MELA_0010 shows evidence of BFB with loss of telomeric region and inversions with increased copy number. **d**, Circos plot of MELA_0018 shows a cluster of structural rearrangements on chromosomes 5 and 18. **e**, **f**, The cluster of rearrangements in (**e**) MELA_0018 on chromosome 5 and (**f**) chromosome 18 are shown from top to bottom: translocations, all other rearrangements, copy number status, log(R ratio) and B-allele frequency.

© 2017 Macmillan Publishers Limited, part of Springer Nature. All rights reserved.

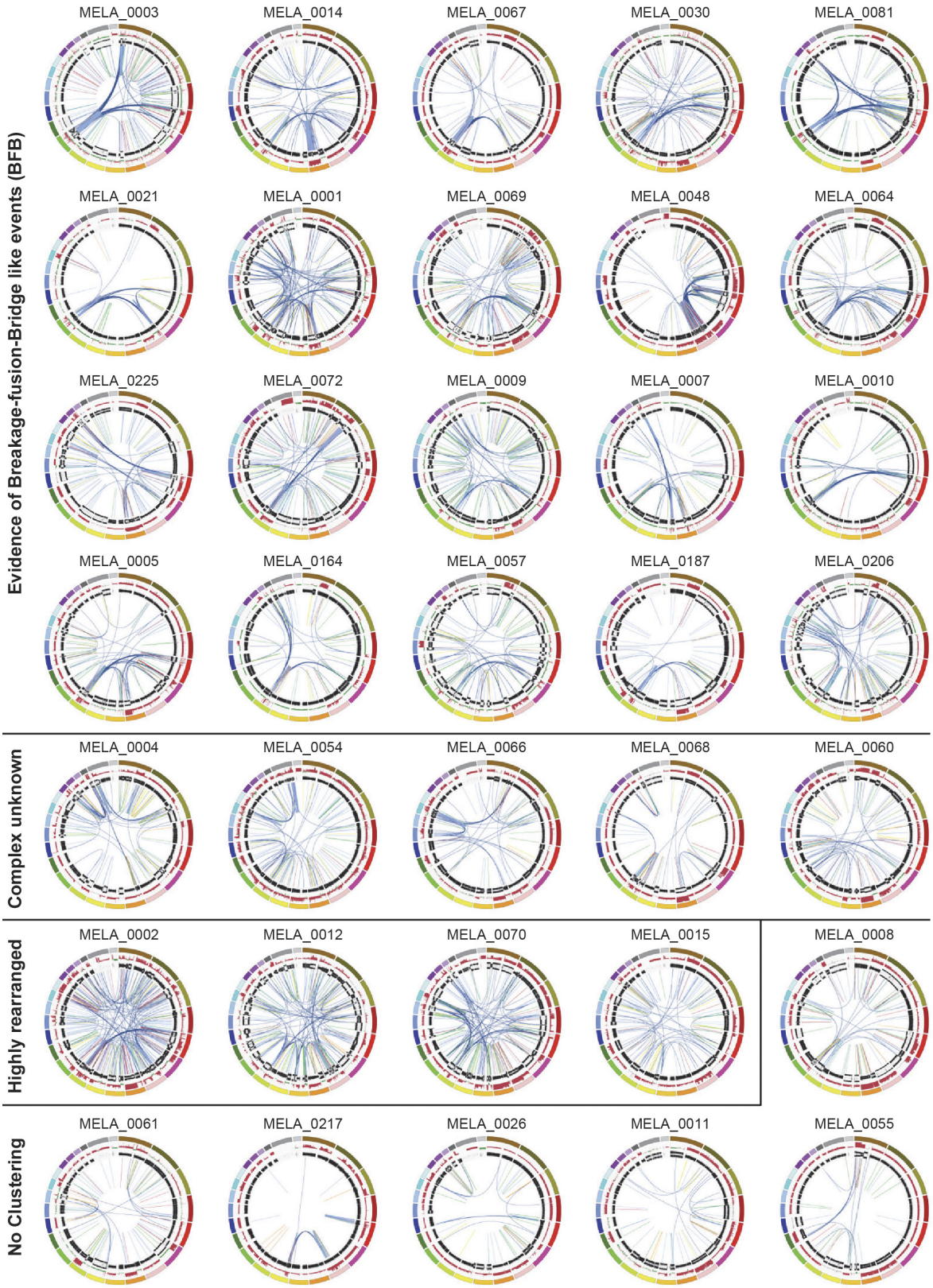

Extended Data Figure 5 | Complex structural rearrangements are frequent in acral melanomas. Circos plots are shown for all acral melanomas ($n = 35$) in the study. The outer coloured ring on the Circos plot represents each chromosome, the next ring is the copy number (red, gain; green, loss), the inner ring is the B-allele frequency, and the structural variants are shown by the lines in the centre of the plot. Tumours that contain BFB events, complex rearrangements, highly rearranged genomes or those that contain no clusters of structural variants are indicated.

© 2017 Macmillan Publishers Limited, part of Springer Nature. All rights reserved.

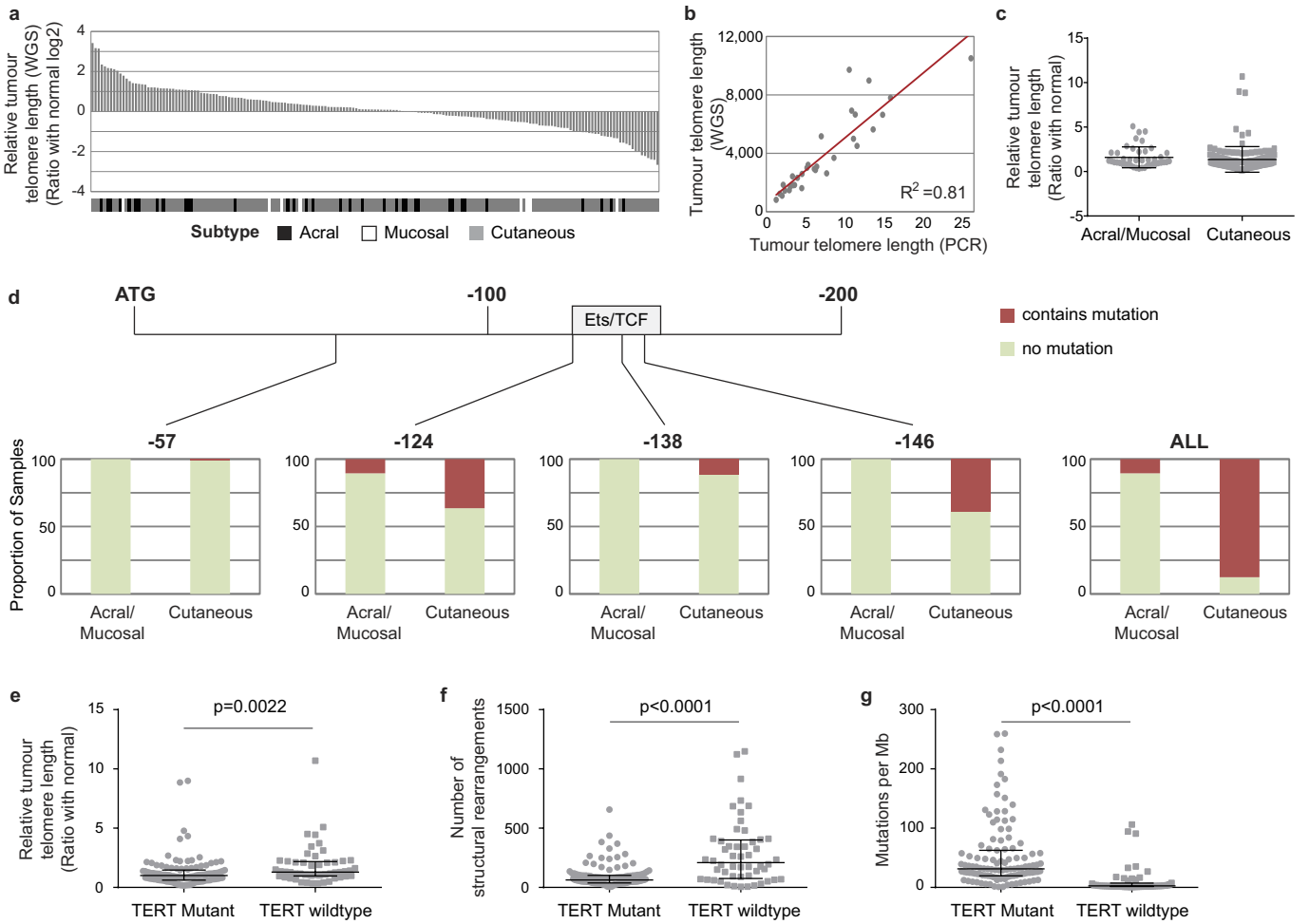

Extended Data Figure 6 | Telomere length and *TERT* promoter mutations. a, The relative melanoma telomere length in each tumour compared with the matched normal ($n = 183$). **b**, Verification of telomere length in 31 samples by PCR. **c**, The telomere length was not associated with melanoma subtype (cutaneous, $n = 140$; acral or mucosal, $n = 43$). **d**, Somatic mutations in the promoter of the *TERT* gene were detected by WGS and/or by capillary sequencing. Mutations were found at −57, −124, −138 and −146 from the ATG site. **e**–**g**, Tumours with *TERT* promoter mutations were associated with (Mann–Whitney *U*-test) (**e**) telomere length, (**f**) the number of structural rearrangements and (**g**) the number of mutations per megabase.

© 2017 Macmillan Publishers Limited, part of Springer Nature. All rights reserved.

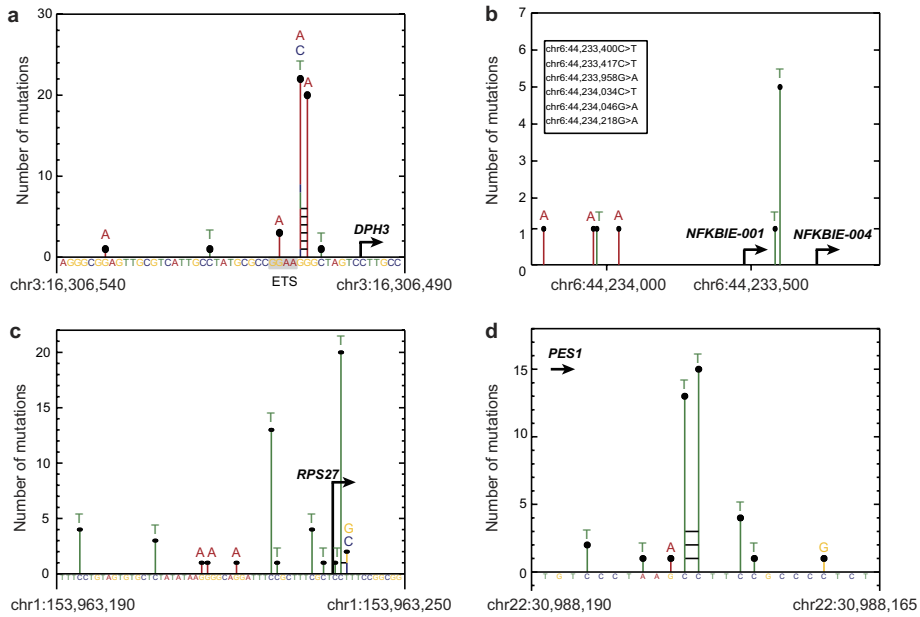

Extended Data Figure 7 | Recurrent *DPH3, NFKBIE, RPS27* and *PES1* promoter mutations. Height and colour of sticks indicate recurrence and mutant base, respectively. Tandem mutations are indicated with black horizontal bars. **a**, Recurrent mutations in promoter of *DPH3* at loci 8 bp ($n = 20$), 9 bp ($n = 22$) and 12 bp ($n = 3$) upstream from the transcription start site. The ETS transcription factor family core motif is shaded in grey. **b**, Recurrent mutation ($n = 5$) at chr6:44,233,400 in the first exon of *NFKBIE-001* isoform and 129 bases upstream from the transcription start site of *NFKBIE-004*, which typically is the expressed transcript in most tissue, including melanoma. Four novel mutations were identified a further 500 kb upstream. **c**, Recurrent mutations on and upstream from the transcription start site of *RPS27*. **d**, Recurrent mutations upstream of *PES1*.

© 2017 Macmillan Publishers Limited, part of Springer Nature. All rights reserved.

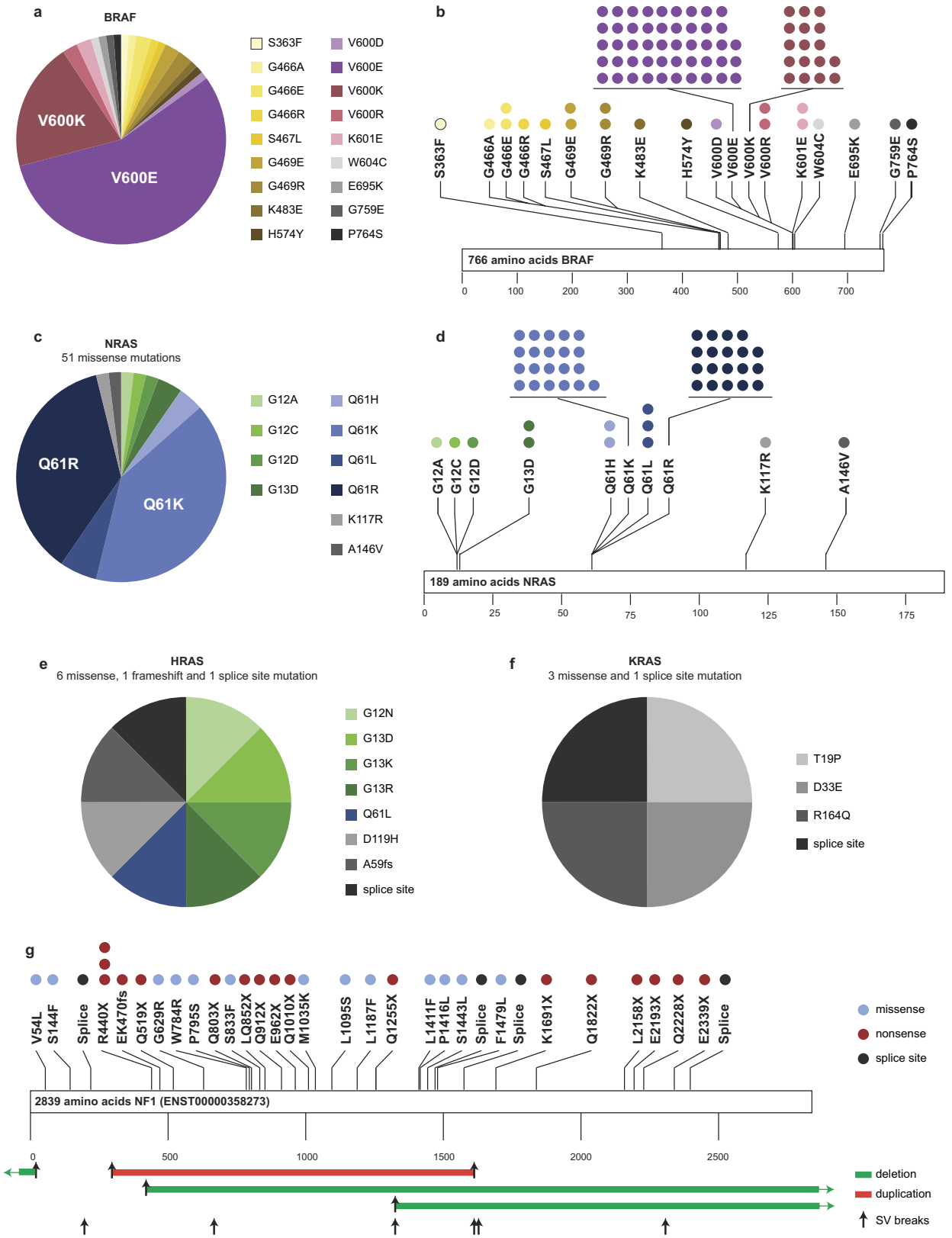

Extended Data Figure 8 | *BRAF*, *RAS* and *NF1* mutations. a, **b**, *BRAF* somatic mutations were identified in 86 of the 183 samples (47%). V600E substitutions accounted for 48 (56%) of these mutations. Other activating mutations at codons 600 and 601 were less frequent (V600K, $n = 17$; V600R, $n = 2$; V600D, $n = 1$; K601E, $n = 2$). **c**, **d**, *NRAS* was mutated in 51 (28%) tumours; 49 of these mutations occurred at 'hotspot' codons 12, 13 or 61. **e**, *HRAS* mutations occurred in eight tumours, five of which were in 'hotspot' codons 12, 13 or 61. **f**, *KRAS* mutations occurred in four tumours, but none occurred at the commonly activating hotspot codons. **g**, *NF1* aberrations occurred throughout the gene in 32 of 183 (17%) tumours and included point mutations/small indels only (15 nonsense, 1 frameshift, 3 splice site and 4 missense). Structural variants predicted to cause loss of function were frequent within *NF1* (structural variant breakpoints indicated by reverse arrows). Some rearrangements were associated with a copy number change (green, loss; red, gain).

© 2017 Macmillan Publishers Limited, part of Springer Nature. All rights reserved.

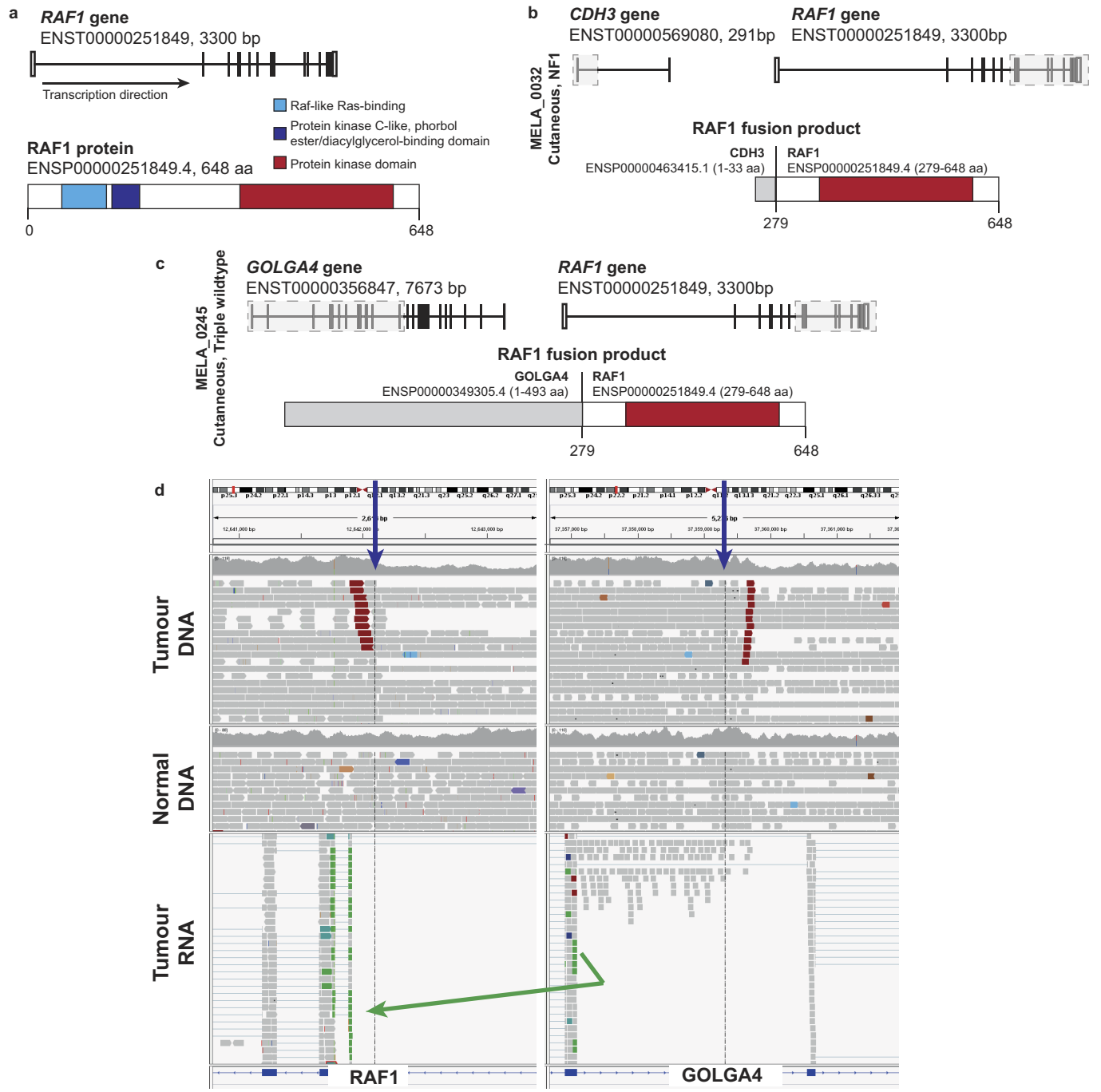

Extended Data Figure 9 | Candidate *RAF1* gene fusions. WGS data were used to identify genomic rearrangements that could result in a gene fusion product. **a**, The *RAF1* gene and protein are shown. **b**, A *RAF1* gene fusion was detected with a small transcript of *CDH3*. The gene fusion is expected to produce a protein that retains the ref1 kinase domain. **c**, A *RAF1–GOLGA4* gene fusion was detected, which is expected to produce a protein that retains the ref1 kinase domain. **d**, Integrative Genomics Viewer view of *RAF1–GOLGA4* gene fusion. DNA breakpoints (purple arrows) are marked by discordantly aligned red coloured read pairs that are in an incorrect orientation and too far apart. There is no matching evidence observed in the normal control sample. Supportive evidence for an expressed gene fusion is visible in RNA sequencing data (bottom horizontal panel) where discordantly aligned reads are highlighted in turquoise and the orientation of a junction fusion between exon 11 of *GOLGA4* and exon 8 of *RAF1* is indicated by the green arrow.

© 2017 Macmillan Publishers Limited, part of Springer Nature. All rights reserved.

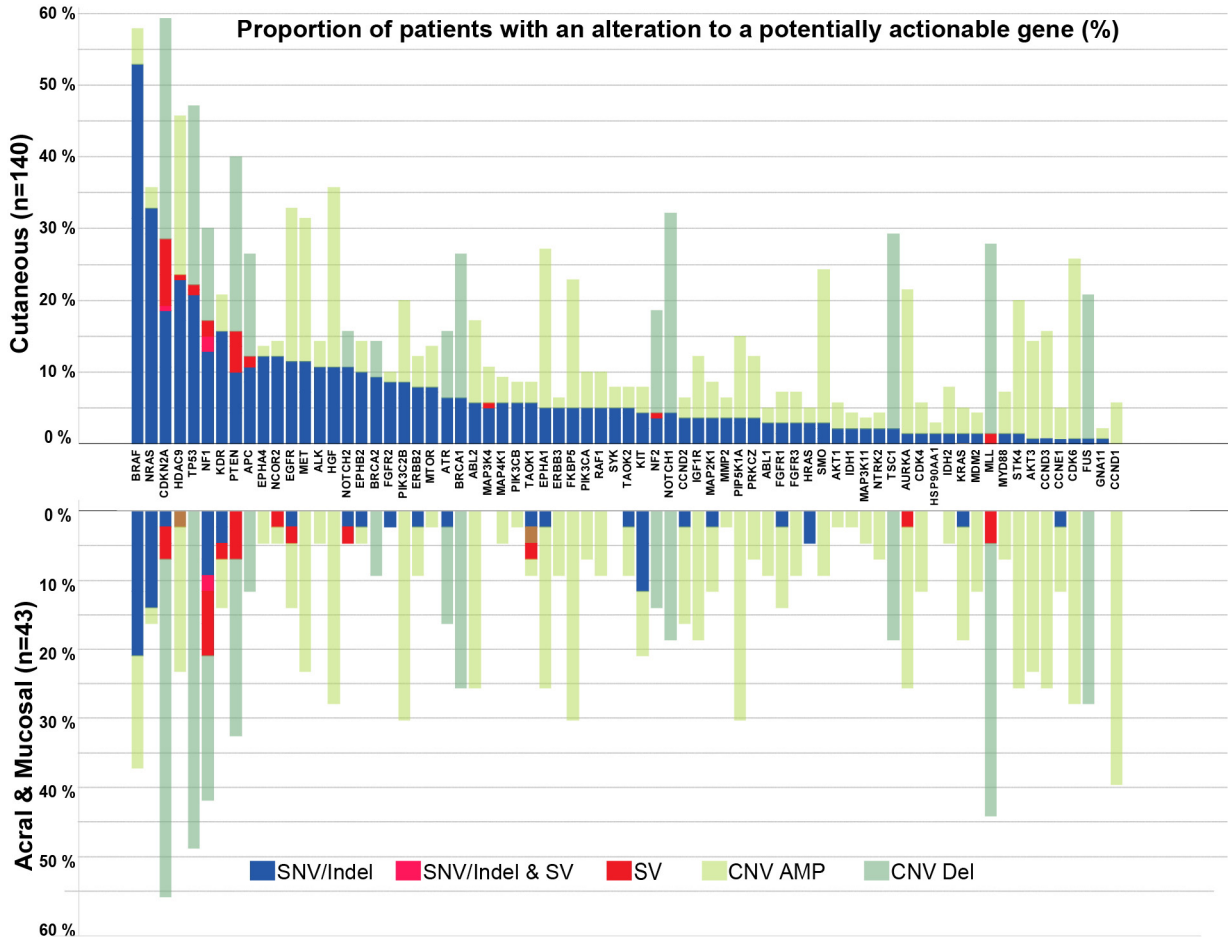

Extended Data Figure 10 | Alterations to potentially actionable genes in cutaneous and non-cutaneous melanomas. Proportion of samples with a somatic variant containing a gene that confers sensitivity to a US Food and Drug Administration-approved or therapeutic agent being used in a clinical trial (in any cancer): non-silent substitution or indel (SNV/indel; dark blue); both SNV/indel and structural variants (light red); structural variants only (dark red) or copy number variation, high-level amplification (green); and deletions (light blue). Genes are ordered by the difference between the frequencies of mutated genes (excluding copy number variation) in cutaneous ($n = 140$) versus non-cutaneous ($n = 43$) melanomas, with genes with a higher mutation frequency in cutaneous melanomas on the left.

© 2017 Macmillan Publishers Limited, part of Springer Nature. All rights reserved.